Phenomenology of the nMSSM from colliders to cosmology

Csaba Balázs,[abc] **Marcela Carena,**[c] **Ayres Freitas**[d] **and Carlos E.M. Wagner**[be]

[a]*School of Physics, Monash University,*
Melbourne VIC 3800, Australia
[b]*HEP Division, Argonne National Laboratory,*
9700 Cass Ave., Argonne, IL 60439, U.S.A.
[c]*Fermi National Accelerator Laboratory,*
P.O. Box 500, Batavia, IL 60510, U.S.A.
[d]*Institut für Theoretische Physik, Universität Zürich,*
Winterthurerstrasse 190, 8057 Zürich, Switzerland
[e]*Enrico Fermi Institute and Kavli Institute for Cosmological Physics,*
Department of Physics, University of Chicago,
5640 S. Ellis Ave., Chicago, IL 60637, U.S.A.
E-mail: `csaba.balazs@sci.monash.edu.au`, `carena@fnal.gov`,
`afreitas@physik.unizh.ch`, `cwagner@hep.anl.gov`

ABSTRACT: Low energy supersymmetric models provide a solution to the hierarchy problem and also have the necessary ingredients to solve two of the most outstanding issues in cosmology: the origin of dark matter and baryonic matter. One of the most attractive features of this framework is that the relevant physical processes are related to interactions at the weak scale and therefore may be tested in collider experiments in the near future. This is true for the Minimal Supersymmetric Standard Model (MSSM) as well as for its extension with the addition of one singlet chiral superfield, the so-called nMSSM. It has been recently shown that within the nMSSM an elegant solution to both the problem of baryogenesis and dark matter may be found, that relies mostly on the mixing of the singlet sector with the Higgs sector of the theory. In this work we review the nMSSM model constraints from cosmology and present the associated collider phenomenology at the LHC and the ILC. We show that the ILC will efficiently probe the neutralino, chargino and Higgs sectors, allowing to confront cosmological observations with computations based on collider measurements. We also investigate the prospects for a direct detection of dark matter and the constraints imposed by the current bounds of the electron electric dipole moment in this model.

KEYWORDS: Extended Supersymmetry, Supersymmetry Phenomenology, Cosmology of Theories beyond the SM, Baryogenesis.

Contents

1. Introduction

In spite of the excellent agreement of the predictions of the Standard Model (SM) with experimental observables, there is still a strong physical motivation for the presence of new physics at the weak scale. The main reason is the belief that the Higgs mechanism of the SM is only an effective description of a more fundamental mechanism of electroweak symmetry breaking, in which the origin and stability of the electroweak scale must be explained. Supersymmetric extensions of the SM [1, 2] allow such a mechanism. In the simplest extensions of the SM, the theory remains perturbative up to scales of the order of the Planck scale and the weak scale is stable under quantum corrections at all orders in perturbation theory. Moreover, the electroweak symmetry is broken radiatively, providing a correlation between the weak scale and the soft supersymmetry breaking scale.

Another strong motivation is a solution to the problem of dark matter. If a discrete symmetry, R-Parity, is imposed in the theory, the lightest supersymmetric particle (LSP) is stable. In the simplest models, it is also neutral and weakly interacting, with an annihilation cross section of the order of the one necessary for the LSP to become a good dark matter candidate.

It has been also realized that supersymmetry may also lead to a solution of another outstanding cosmological problem, namely, the baryon-antibaryon asymmetry [3, 4]. In the MSSM, a solution to this problem by weak scale physics demands a light stop as well as non-vanishing CP-violating phases in the chargino-neutralino sector. The presence of a light stop, with mass smaller than the top quark mass, tends to push the lightest CP-even Higgs mass to values close to the ones restricted by experimental searches. Therefore, this scenario is highly constrained and it will be probed at the Tevatron and the LHC colliders in the near future, as well as in electric dipole moment and direct dark matter searches [5, 6] and the ILC [7]. Supersymmetry also plays a relevant role for the generation of the baryon asymmetry in the so-called soft leptogenesis scenario, which again demands very specific values for the soft supersymmetry breaking parameters in the neutrino sector [8], which can be naturally obtained only in certain supersymmetry breaking scenarios [9].

A less constrained solution to the baryon asymmetry may be found within extensions of the MSSM with additional chiral singlet superfields. In particular, it has been recently shown that a particularly simple extension of the MSSM, the so-called nMSSM [10 – 14] includes all the relevant properties to lead to a successful generation of the baryon asymmetry at the weak scale [15, 16], without the need of light squarks and with values of the lightest CP-even Higgs mass which are naturally above the current experimental bound [17].

One interesting feature of the nMSSM is that the lightest neutralino is usually an admixture of the fermion component of the singlet field and the Higgsinos. Due to the absence of explicit mass terms in the Higgsino-singlino sector, its mass is bounded to be below 70 GeV. A relaxation of this upper bound may only be obtained by allowing the trilinear Higgs-singlet coupling to become strong at scales lower than the Grand Unification (GUT) scale, as happens in the so-called fat Higgs models and gauge extensions[1] of the

---

[1]Such gauge extensions open new possibilities for baryogenesis [19], but this possibility will not be pursued any further in this paper.

nMSSM [18]. In this work, we shall demand perturbative consistency of the theory up to the GUT scale, and therefore the aforementioned bound applies. For light neutralinos, the annihilation cross section is dominated by s-channel Z^0 boson exchange and a neutralino relic density consistent with all experimental bounds, may only be obtained for values of the neutralino mass of about 30-45 GeV.

Such a light neutralino has relevant phenomenological consequences. For instance, the lightest CP-even Higgs tends to decay predominantly into neutralinos, leading to invisible signatures at hadron and lepton colliders [16]. Moreover, one of the predictions of this model is the presence of relatively light charginos and neutralinos with masses smaller than about 200 GeV. Detection of these weakly interacting particles at hadron colliders becomes difficult if there are no strongly interacting superpartners with masses below the TeV scale. Assuming that the relevant CP-violating phases are in the gaugino masses, successful baryogenesis may be easily achieved for weak-scale gaugino masses of the order of 100-300 GeV, and at least one relatively light squark in order to avoid the so-called Giudice-Shaposhnikov suppression of chiral charges [20]. We will assume the presence of top and bottom squarks with masses of order of 500 GeV, and the presence of a gluino with mass dictated by the gaugino mass unification condition. The phenomenological properties at hadron colliders depend strongly on these last assumptions.

In addition to discussing the prospects for discovery of the light Higgs and superpartner states at the LHC, we will perform a detailed phenomenological analysis of nMSSM physics at the ILC. In this case the values of the strongly interacting particle masses become less important. The same is true for the analysis of the direct dark matter detection properties and the constraints coming from the bounds on the electron electric dipole moments that we investigate in this work.

The article is organized as follows. In section 2 we present an overview of the nMSSM and present experimental constraints to define a benchmark scenario for the model. In section 3 we analyze the corresponding collider phenomenology at the LHC and the ILC, which we then connect with the cosmology constraints related to the dark matter relic density and baryogenesis in section 4. In particular, we present the constraints coming from direct searches of dark matter and the non-observation of an electron electric dipole moment. We reserve section 5 for our conclusions.

2. General properties of and constraints on the nMSSM

2.1 Overview

One of the original motivations for a singlet extension of the MSSM is the difficulty to explain why the μ-parameter in the superpotential is of order of the electroweak scale, instead of the GUT or Planck scale. This problem is circumvented by introducing a singlet chiral superfield $\hat{S}$, and generating a weak-scale μ-parameter through the vacuum expectation value of the scalar component S of the singlet. This requires the inclusion of a triple-Higgs coupling term

$$W_\lambda = \lambda \hat{S} \hat{H}_1 \cdot \hat{H}_2 \qquad (2.1)$$

in the superpotential, where $\hat{H}_{1,2}$ are the superfields of the two Higgs doublets,

$$\hat{H}_1 = \begin{pmatrix} H_1^0 \\ H_1^- \end{pmatrix}, \qquad\qquad \hat{H}_2 = \begin{pmatrix} H_2^+ \\ H_2^0 \end{pmatrix}. \qquad (2.2)$$

This triple-Higgs coupling also helps to push up the mass of the CP-even Higgs boson responsible for electroweak symmetry breaking, so that the bound from LEP, $m_{\mathrm{h}^0} \gtrsim 114.4$ GeV [17], can be satisfied without substantial fine tuning. Finally, the new contribution increases the strength of the electroweak phase transition, thus allowing the possibility of electroweak baryogenesis in a large region of parameter space [16].

In a general singlet extension, the superpotential can also contain a triple-self-coupling, a mass term and a tadpole term for $\hat{S}$,

$$\begin{aligned} W_{\mathrm{SMSSM}} = {} & \lambda \hat{S}\hat{H}_1 \cdot \hat{H}_2 + \kappa \hat{S}^3 + m_{\mathrm{N}}\hat{S}^2 + \frac{m_{12}^2}{\lambda}\hat{S} \\ & + y_{\mathrm{u}}\hat{Q} \cdot \hat{H}_2\,\hat{U}^c + y_{\mathrm{d}}\hat{Q} \cdot \hat{H}_1\,\hat{D}^c + y_{\mathrm{e}}\hat{L} \cdot \hat{H}_1\,\hat{E}^c, \end{aligned} \qquad (2.3)$$

where $y_{\mathrm{u,d,e}}$ are the 3×3 Yukawa coupling matrices.

In the Next-to-Minimal Supersymmetric Standard Model (NMSSM), a discrete $\mathbb{Z}_3$ symmetry is imposed, which forbids the tadpole and mass terms and only leaves dimensionless couplings in the superpotential. However, once the singlet scalar acquires a vacuum expectation value, the $\mathbb{Z}_3$ symmetry is broken and unacceptable domain walls can be generated [10, 21].

In the Nearly Minimal Supersymmetric Standard Model (nMSSM) [11 – 14], a $\mathbb{Z}_5$ or $\mathbb{Z}_7$ R-symmetry is introduced in the superpotential and the Kähler potential, which forbids quadratic and cubic self-interactions of the singlet. However, at higher loop orders, a tadpole term is induced due to supergravity effects. It is suppressed at the six ($\mathbb{Z}_5$) or seven ($\mathbb{Z}_7$) loop level, so that it is naturally of weak-scale order and does not destabilize the hierarchy [11 – 13]. The discrete symmetries also ensure that rapid proton decay does not occur, while Majorana neutrino masses are allowed. Furthermore the lightest supersymmetric particle, usually the lightest neutralino, is quasi-stable on cosmological time-scales [16], even without the introduction of R-Parity. The superpotential of the nMSSM is thus

$$\begin{aligned} W_{\mathrm{nMSSM}} = {} & \lambda \hat{S}\hat{H}_1 \cdot \hat{H}_2 + \frac{m_{12}^2}{\lambda}\hat{S} \\ & + y_{\mathrm{u}}\hat{Q} \cdot \hat{H}_2\,\hat{U}^c + y_{\mathrm{d}}\hat{Q} \cdot \hat{H}_1\,\hat{D}^c + y_{\mathrm{e}}\hat{L} \cdot \hat{H}_1\,\hat{E}^c. \end{aligned} \qquad (2.4)$$

In the following, the phenomenological properties of the nMSSM will be analyzed in more detail.

2.2 CP violation

In the nMSSM superpotential, the parameters λ, m_{12} and y_{f} can in general be complex. However, the phase of λ does not generate physical CP-violating effects, since it can be made real by suitable gauge rotations [22]. As in the Standard Model, the Yukawa couplings y_{f} lead to one physical phase in the CKM quark mixing matrix, which is constrained by

	$\hat{H}_1$	$\hat{H}_2$	$\hat{S}$	$\hat{Q}$	$\hat{L}$	$\hat{U}^c$	$\hat{D}^c$	$\hat{E}^c$	$\hat{B}$	$\hat{W}$	$\hat{g}$	W_{nMSSM}
$\mathrm{U}(1)_{\mathrm{R}}$	0	0	2	1	1	1	1	1	0	0	0	2
$\mathrm{U}(1)_{\mathrm{PQ}}$	1	1	-2	-1	-1	0	0	0	0	0	0	0

Table 1: Charges of superfields under the $\mathrm{U}(1)_{\mathrm{R}}$ and $\mathrm{U}(1)_{\mathrm{PQ}}$ symmetries of the superpotential. Note that the $\mathrm{U}(1)_{\mathrm{R}}$ charges of the fermionic components differ by 1 from those of the superfields.

present data from many heavy-flavor experiments. The phase of m_{12}^2 will be addressed below.

Beyond the superpotential, new complex phases can appear through supersymmetry breaking. The soft supersymmetry breaking Lagrangian reads

$$
\begin{aligned}
\mathcal{L}_{\mathrm{soft}} = {} & m_1^2 H_1^\dagger H_1 + m_2^2 H_2^\dagger H_2 + m_s^2 |S|^2 + (t_s S + a_\lambda S H_1 \cdot H_2 + \mathrm{h.c.}) \\
& + (M_1 \widetilde{B}\widetilde{B} + M_2 \widetilde{W} \cdot \widetilde{W} + M_3\, \tilde{g}\tilde{g} + \mathrm{h.c.}) \\
& + m_{\tilde{q}}^2\, \tilde{q}_{\mathrm{L}}^\dagger \cdot \tilde{q}_{\mathrm{L}} + m_{\tilde{u}}^2 |\tilde{u}_{\mathrm{R}}|^2 + m_{\tilde{d}}^2 |\tilde{d}_{\mathrm{R}}|^2 + m_{\tilde{l}}^2\, \tilde{l}_{\mathrm{L}}^\dagger \cdot \tilde{l}_{\mathrm{L}} + m_{\tilde{e}}^2 |\tilde{e}_{\mathrm{R}}|^2 \\
& + (y_{\mathrm{u}} A_{\mathrm{u}}\, \tilde{q}_{\mathrm{L}} \cdot H_2\, \tilde{u}_{\mathrm{R}}^* + y_{\mathrm{d}} A_{\mathrm{d}}\, \tilde{q}_{\mathrm{L}} \cdot H_1\, \tilde{d}_{\mathrm{R}}^* + y_{\mathrm{e}} A_{\mathrm{e}}\, \tilde{l}_{\mathrm{L}} \cdot H_1\, \tilde{e}_{\mathrm{R}}^* + \mathrm{h.c.}).
\end{aligned}
\tag{2.5}
$$

Here $H_i, S, \tilde{q}_{\mathrm{L}}, \tilde{u}_{\mathrm{R}}, \tilde{d}_{\mathrm{R}}, \tilde{l}_{\mathrm{L}}, \tilde{e}_{\mathrm{R}}$ are the scalar components of the superfields $\hat{H}_i, \hat{S}, \hat{Q}, \hat{U}, \hat{D}, \hat{L}, \hat{E}$, where the quark and lepton fields exist in three generations (the generation index has been suppressed in the formula). $\widetilde{B}, \widetilde{W}, \tilde{g}$ denote the fermionic components of the gauge super-multiplets. Among the soft breaking parameters, a_λ, t_{s}, $M_{1,2,3}$ and $A_{\mathrm{u,d,e}}$ can be complex. However not all their phases are physical. To see this, one can observe that the superpotential is invariant under an $\mathrm{U}(1)_{\mathrm{R}}$ symmetry, with the charges listed in table 1. In addition, it obeys an approximate Peccei-Quinn symmetry $\mathrm{U}(1)_{\mathrm{PQ}}$, which is broken by the singlet tadpole term $\propto m_{12}^2$. Both $\mathrm{U}(1)_{\mathrm{R}}$ and $\mathrm{U}(1)_{\mathrm{PQ}}$ are broken by some of the supersymmetry breaking terms.

With the help of the $\mathrm{U}(1)_{\mathrm{R}}$ and $\mathrm{U}(1)_{\mathrm{PQ}}$, the fields can be rotated so that the phases of two parameters become zero. By analyzing the charges, it can be seen that the following products remain invariant under both R- and PQ-transformations:

$$
\begin{aligned}
& \arg(m_{12}^2 t_{\mathrm{s}}^* a_\lambda), \\
& \arg(m_{12}^2 t_{\mathrm{s}}^* M_i), && i = 1, 2, 3, \\
& \arg(m_{12}^2 t_{\mathrm{s}}^* A_{\mathrm{u}}), && (3 \text{ generations}), \\
& \arg(m_{12}^2 t_{\mathrm{s}}^* A_{\mathrm{d}}), && (3 \text{ generations}), \\
& \arg(m_{12}^2 t_{\mathrm{s}}^* A_{\mathrm{e}}), && (3 \text{ generations}),
\end{aligned}
\tag{2.6}
$$

corresponding to 13 physical CP-violating phases in addition to the CKM phase. Without loss of generality, the phases of m_{12} and t_{s} can be chosen real, so that the physical phases are transferred into a_λ, $M_{1,2,3}$ and $A_{\mathrm{u,d,e}}$.

In this work, for simplicity, gaugino unification is assumed, so that $M_1 : M_2 : M_3 \approx 1 : 2 : 6$. In this case, the gaugino masses carry one common phase, $\phi_{\mathrm{M}_1} = \phi_{\mathrm{M}_2} = \phi_{\mathrm{M}_3} \equiv \phi_{\mathrm{M}}$. To simplify the analysis further, the phases in $A_{\mathrm{u,d,e}}$ and a_λ are set to zero.

2.3 Higgs sector

The scalar potential at tree-level receives contributions from F-, D-terms and soft supersymmetry breaking. To avoid charge and color breaking vacuum solutions and unacceptably large neutrino masses, the squarks and sleptons must not receive vacuum expectation values. In this case, the Higgs potential at tree-level reads

$$V_0 = V_{\text{F}} + V_{\text{D}} + V_{\text{soft}}, \tag{2.7}$$

$$V_{\text{F}} = \left| \lambda H_1 \cdot H_2 + \frac{m_{12}^2}{\lambda} \right|^2 + |\lambda S|^2 (H_1^\dagger H_1 + H_2^\dagger H_2), \tag{2.8}$$

$$V_{\text{D}} = \frac{\bar{g}^2}{8}(H_1^\dagger H_1 - H_2^\dagger H_2)^2 + \frac{g^2}{2}|H_1^\dagger H_2|^2, \tag{2.9}$$

$$V_{\text{soft}} = m_1^2 H_1^\dagger H_1 + m_2^2 H_2^\dagger H_2 + m_{\text{s}}^2 |S|^2 + (t_{\text{s}} S + a_\lambda S H_1 \cdot H_2 + \text{h.c.}), \tag{2.10}$$

where $\bar{g}^2 = g^2 + g'^2$, and g, g' are the SU(2), U(1) gauge couplings, respectively. As mentioned in the previous section, we constrain all parameters in the Higgs sector to be real. Nevertheless, we allow complex phases in the gaugino sector, which in turn would generate small CP-violating phases in the Higgs sector through radiative corrections. However, the effect of gaugino loop contributions to the Higgs effective potential is generally subdominant, compared to the top-stop loops, and thus can be neglected in the following discussion.

In the zero-temperature vacuum state, the neutral Higgs components acquire non-zero vacuum expectation values,

$$\langle S \rangle = v_{\text{s}}, \qquad \langle H_1^0 \rangle = v_1, \qquad \langle H_2^0 \rangle = v_2. \tag{2.11}$$

It is useful to define $\tan \beta = v_2/v_1$. The minimization conditions for electroweak symmetry breaking give at Born level

$$m_1^2 = -(m_{12}^2 + a_\lambda v_{\text{s}})\frac{v_2}{v_1} - \frac{\bar{g}^2}{4}(v_1^2 - v_2^2) - \lambda^2(v_2^2 + v_{\text{s}}^2), \tag{2.12}$$

$$m_2^2 = -(m_{12}^2 + a_\lambda v_{\text{s}})\frac{v_1}{v_2} - \frac{\bar{g}^2}{4}(v_2^2 - v_1^2) - \lambda^2(v_1^2 + v_{\text{s}}^2), \tag{2.13}$$

$$m_{\text{s}}^2 = -a_\lambda \frac{v_1 v_2}{v_{\text{s}}} - \frac{t_{\text{s}}}{v_{\text{s}}} - \lambda^2 v^2. \tag{2.14}$$

The physical mass eigenstates of the Higgs sector consist of three neutral CP-even scalars $S_{1,2,3}$, two neutral CP-odd scalars $P_{1,2}$ and one charged scalar $H^\pm$. Both the CP-even and CP-odd neutral scalars share a component of the singlet scalar S.

In the sector of the CP-odd scalars, one combination of the two doublets form the Goldstone mode G^0, which is absorbed into the longitudinal mode of the Z boson. The other linear combination of the two doublets, A^0, mixes with the imaginary part of the singlet S to give the two physical states. In the basis $(A^0, \Im m\, S)$, their mass matrix reads

$$M_{\text{P}}^2 = \begin{pmatrix} M_{\text{A}}^2 & -a_\lambda v \\ -a_\lambda v & m_{\text{s}}^2 + \lambda^2 v^2 \end{pmatrix}, \tag{2.15}$$

where

$$M_A^2 = -\frac{2}{s_{2\beta}}(m_{12}^2 + a_\lambda v_s),$$
(2.16)

and $s_{2\beta} = \sin 2\beta$. The mass eigenstates $P_{1,2}$ are related to this basis by the mixing matrix O^P,

$$\begin{pmatrix} P_1 \\ P_2 \end{pmatrix} = O^P \begin{pmatrix} A^0 \\ \Im m\, S \end{pmatrix}.$$
(2.17)

For large values of M_A, corresponding to large negative values of m_{12}^2, the mixing between the two CP-odd scalars is relatively small, with the light pseudo-scalar P_1 being almost completely singlet, while the heavy pseudo-scalar P_2 has a very small singlet component and a mass of about $m_{P_2} \sim M_A$. These properties have strong consequences for Higgs searches at LHC and ILC, as discussed in the next section.

Similarly to the CP-odd sector, the CP-even Higgs eigenstates are related to the doublet and singlet components by the mixing matrix O^S,

$$\begin{pmatrix} S_1 \\ S_2 \\ S_3 \end{pmatrix} = O^S \begin{pmatrix} H_1^0 \\ H_2^0 \\ \Re e\, S \end{pmatrix}.$$
(2.18)

For $M_A \ll M_Z$, there are one heavy mass eigenstate S_3 with small singlet component, and two light eigenstates S_1, S_2 with sizable singlet and doublet admixtures.

The Higgs potential receives large radiative corrections, with the dominant contribution stemming from top-stop loops. These effects have been calculated in ref. [23, 13] and are included in this work.

The influence of the parameter λ gives an additional positive contribution to the mass of the lightest Higgs boson, so that the bound of about $114\,\mathrm{GeV}$ from LEP can be easily avoided even for moderate values of $\tan\beta$ and stop mass eigenvalues $m_{\tilde{t}_1}, m_{\tilde{t}_2}$. From the vacuum expectation value of S, v_s, an effective μ-parameter is generated, $\mu = -\lambda v_s$.

2.4 Chargino and neutralino sector

The presence of the fermion component of the singlet superfield, the singlino $\tilde{S}$, leads to a fifth neutralino state. The chargino mass matrix in the basis $(\widetilde{W}^\pm, \widetilde{H}^\pm)$ is

$$M_{\tilde\chi^\pm} = \begin{pmatrix} M_2 & \sqrt{2}s_\beta M_W \\ \sqrt{2}c_\beta M_W & -\lambda v_s \end{pmatrix},$$
(2.19)

while the neutralino mass matrix in the basis $(\widetilde{B}^0, \widetilde{W}^0, \widetilde{H}_1^0, \widetilde{H}_2^0, \widetilde{S})$ is given by

$$M_{\tilde\chi^0} = \begin{pmatrix} M_1 & 0 & -c_\beta s_W M_Z & s_\beta s_W M_Z & 0 \\ 0 & M_2 & c_\beta c_W M_Z & -s_\beta c_W M_Z & 0 \\ -c_\beta s_W M_Z & c_\beta c_W M_Z & 0 & \lambda v_s & \lambda v_2 \\ s_\beta s_W M_Z & -s_\beta c_W M_Z & \lambda v_s & 0 & \lambda v_1 \\ 0 & 0 & \lambda v_2 & \lambda v_1 & 0 \end{pmatrix},$$
(2.20)

where the abbreviations $s_\beta \equiv \sin\beta$, $c_\beta \equiv \cos\beta$, $s_W \equiv \sin\theta_W$, $c_W \equiv \cos\theta_W$ have been used. The neutralino mass matrix is diagonalized by a unitary matrix N, such that

$$N^* M_{\tilde{\chi}^0} N^\dagger = \text{diag}(m_{\tilde{\chi}_1^0}, m_{\tilde{\chi}_2^0}, m_{\tilde{\chi}_3^0}, m_{\tilde{\chi}_4^0}, m_{\tilde{\chi}_5^0}). \tag{2.21}$$

Perturbativity of the trilinear coupling λ up to the GUT scale requires that $\lambda \lesssim 0.8$ [16]. For values of $\lambda < 0.8$, the lightest neutralino has a large singlino component, and a mass below about $60\,\text{GeV}$.

2.5 Experimental and astrophysical constraints

The chargino and neutralino spectrum is constrained by new physics searches at LEP. For the lightest chargino, the LEP measurements lead to the constraint $m_{\tilde{\chi}_1^\pm} > 104\,\text{GeV}$ or $\sigma[e^+ e^- \to \tilde{\chi}_1^+ \tilde{\chi}_1^-] \times \text{BR} < 10\,\text{fb}$, where σ is the production cross section at $\sqrt{s} = 208\,\text{GeV}$, and BR the branching ratio into hadron or leptons. Similarly, the corresponding requirement for neutralinos is $(m_{\tilde{\chi}_1^0} + m_{\tilde{\chi}_2^0}) > 208\,\text{GeV}$ or $\sigma[e^+ e^- \to \tilde{\chi}_1^0 \tilde{\chi}_2^0] \times \text{BR} < 10\,\text{fb}$ [24]. Moreover, if the lightest neutralino is so light that $m_{\tilde{\chi}_1^0} < M_Z/2$, the measurement of the total Z-boson width imposes the limit $\text{BR}[Z \to \tilde{\chi}_1^0 \tilde{\chi}_1^0] < 0.8 \times 10^{-3}$ [25]. On the other hand, if the nMSSM is to account for the dark matter relic density in the universe, the lightest neutralino mass is bound to be in the range $25\,\text{GeV} < m_{\tilde{\chi}_1^0} < 40\,\text{GeV}$ [16].

For the mechanism of electroweak baryogenesis to work successfully, the electroweak phase transition needs to be strongly first order, and new sources of CP-violation beyond the CKM matrix must be present. The electroweak phase transition can be made first order through a relatively large cubic term in the effective Higgs potential. In the nMSSM, similar to other singlet extensions of the MSSM, this cubic term is realized at tree-level by the a_λ soft breaking parameter. As a consequence, a strongly first order phase transition can be achieved without relying on radiative contributions from a light stop as in the MSSM [16, 27, 26]. As a result, neither of the stop masses is constrained to be small ($\lesssim 150\,\text{GeV}$ in the MSSM), but rather can amount to several hundred GeV.

CP-violation in baryon-number violating processes can be introduced via complex couplings in the Higgs sector or through complex parameters in currents that couple sufficiently strongly to the Higgs potential. In the nMSSM, four physical phases can thus contribute to the baryon asymmetry, the phases of M_1, M_2, A_t and t_s [27]. In this work, as emphasized before, it is assumed that the only non-zero phase (besides the CKM matrix) is a common phase of the gaugino masses, $\phi_{M_1} = \phi_{M_2} = \phi_{M_3} \equiv \phi_M$.

In the presence of CP-violating phases, the nMSSM parameter space is constrained by the experimental limits on the electric dipole moment (EDM) of the electron, neutron and ^{199}Hg nucleus [28, 29]. The upper bound on the electron EDM is derived from limits of the EDM of the ^{205}Tl atom. For the phases considered in this work, without mixing between the CP-even and CP-odd Higgs states, the CP-odd electron-neutron operator studied in [30] vanishes, and the ^{205}Tl EDM is due almost entirely to the electron EDM. This translates into a limit on the electron EDM of [28]

$$|d_e| < 1.9 \times 10^{-27} \, e\,cm, \tag{2.22}$$

at 95% CL.

The electron EDM receives potentially large contributions from one-loop sfermion-gaugino diagrams [31], which become small for large masses of several TeV for the first two generation sleptons. A similar role is played by the squarks in the EDMs of the neutron and Hg atom. Two-loop contributions from diagrams with charginos and charged Higgs propagators can also be sizable, but just as in the MSSM [32] they can be suppressed below the current limits for sizable values of the pseudo-scalar masses and $\tan\beta \sim \mathcal{O}(1)$. However, since the two-loop contributions are enhanced by the same complex phase that generates the baryon asymmetry, the electron EDM bound presents a particularly severe constraint on electroweak baryogenesis.

The one- and two-loop contributions to the electron EDM were calculated following refs. [32] and [33, 30], respectively. In the calculation of the one- and two-loop electron EDM contributions, we have included the Higgs and slepton mixing.

Note that while slepton mixing is suppressed with the very small electron mass, the overall contribution to the electron EDM requires a spin flip and is thus also proportional the electron mass. As a result, slepton mixing can lead to non-negligible effects when the slepton masses are moderate. On the other hand, the contribution from the heaviest of the Higgs states S_3 and P_2 is suppressed due to their large masses.

For first and second generation sfermion masses of about $10\,\text{TeV}$, pseudo-scalar mass M_A higher than $500\,\text{GeV}$, and values of $\tan\beta \sim \mathcal{O}(1)$, which is in accordance with baryogenesis constraints, we find that phases $\phi_M \sim \mathcal{O}(1)$ are allowed by the electron and neutron EDM constraints. Since a sufficiently large baryon asymmetry could be generated for phases in the range $\phi_M \sim 0.1\ldots0.3$ [16],[2] this leaves a large window for this scenario to be realized in the nMSSM.

Here we do not attempt to provide a theoretical model that can explain this pattern for the superpartner masses and parameters, but it has been pointed out in the literature that a roughly similar pattern might emerge within the framework of split supersymmetry [38].

2.6 Benchmark scenario A

In the following sections, the collider phenomenology and dark matter detection expectation will be analyzed in detail for the concrete parameter point A from ref. [16]. The parameters of this scenario are summarized in table 2. To avoid EDM constraints, the sleptons and squarks of the first two generations have masses of $10\,\text{TeV}$ in benchmark scenario A. In contrast, the masses of the third generation sfermions are assumed to be around $500\,\text{GeV}$. There are no strong bounds for these masses, but stop masses with a few hundred GeV are favored by Higgs mass naturalness and baryogenesis. The masses and decay modes of

---

[2]Different methods have been used to compute the baryon asymmetry in the MSSM [34–37]. The values derived in ref. [16] are based on the method of ref. [34]. While other methods [36] tend to lead to a higher baryon asymmetry, a more recent calculation leads to a lower one [37]. Furthermore, there are several approximations performed in the computation of the baryon asymmetry, leading to an uncertainty, of order one, on the necessary CP-violation phases required for the realization of this scenario. In section 4.3.2, we provide a more general discussion of the possible sources of CP-violation, and how they affect the phenomenology of this model.

$\tan\beta$	λ	$v_{\rm s}$	a_λ	$t_{\rm s}^{1/3}$	$M_{\rm A}$	$|M_1|$	$|M_2|$	$|M_3|$	$\phi_{\rm M}$	
1.7	0.619	-384	373	157	923	122.5	245	730	0.14	
$m_{Q1,2}$	$m_{U1,2}$	$m_{D1,2}$	$m_{L1,2}$	$m_{E1,2}$	m_{Q3}	m_{U3}	m_{D3}	m_{L3}	m_{E3}	$A_{\rm t,b,\tau}$
10000	10000	10000	10000	10000	500	500	500	500	500	-100

Table 2: Parameters for the reference point A [16] used in this study. All dimensionful parameters are given in GeV.

the neutralinos, charginos, Higgs scalars, third generation squarks and the gluino for this scenario are listed in table 3, table 4 and table 5.

The relatively light neutralino and chargino spectrum is typical for a nMSSM scenario that is in agreement with electroweak baryogenesis and the relic dark matter density [16]. The lightest neutralino has a large singlino component, so that the bound from the invisible Z-boson width is evaded although $m_{\tilde\chi_1^0} < M_{\rm Z}/2$. Nevertheless, the dark matter annihilation cross-section is dominated by s-channel Z exchange, since the combined mass of two $\tilde\chi_1^0$ is close to the Z resonance, $2m_{\tilde\chi_1^0} \sim M_{\rm Z}$. As the sfermions are relatively heavy, the other neutralino and chargino states mainly decay through gauge bosons.

Owing the small mass of the lightest neutralino $\tilde\chi_1^0$, the light Higgs scalars S_1, S_2 and P_1 decay predominantly into two $\tilde\chi_1^0$. For the light CP-odd scalar P_1, which is an almost pure singlino state, this is essentially the only allowed channel, with all other contributions being far below 1% and thus negligible.

Since the most relevant contribution to the annihilation cross section is coming from the Z pole, in ref. [16] a simple calculation sufficed to determine the relic abundance of neutralinos for the benchmark cases.[3] Due to the precision nature that the ILC lends to our present work, we paid careful attention to reproducing, and improving, the earlier results. In our work, we include an improved superpartner spectrum calculation, all possible co-annihilation channels, all SM final states, and solve the relevant Boltzmann equation numerically for the relic density calculation.

While our numbers closely agree with those of ref. [16] there are some small deviations. Notably, our relic density calculation results in slightly higher values. When using the input values for benchmark A, we obtain a neutralino relic density of $\Omega h^2 = 0.131$. The deviation of this from the latest WMAP central value $\Omega h^2 = 0.111$ [39] is comparable to the other theoretical and experimental uncertainties (higher order corrections to sparticle masses and annihilation cross sections, systematic errors, etc.) entering into this calculation.

To demonstrate the uncertainty in the relic density calculation, we note that a variation of the neutralino mass by less than $1\,{\rm GeV}$ is enough to change the relic density by 0.025 for scenario A. Since the main focus of our work is collider phenomenology and a $1\,{\rm GeV}$ shift in the neutralino mass affects collider phenomenology negligibly, our results remain valid for all values close to $\Omega h^2 = 0.111$.

Therefore, in spite of the discrepancy in Ωh^2, we will stick to the scenario A in our numerical analysis.

---

[3] We thank A. Menon and D. Morrissey to provide us with their original codes.

Sparticle	Mass m [GeV]	Width Γ [GeV]	Decay modes	
$\tilde{\chi}_1^0$	33.3	—	—	
$\tilde{\chi}_2^0$	106.6	0.00004	$\tilde{\chi}_2^0 \to Z^* \tilde{\chi}_1^0$	100%
$\tilde{\chi}_3^0$	181.5	0.09	$\tilde{\chi}_3^0 \to Z \tilde{\chi}_1^0$	74%
			$\to S_1 \tilde{\chi}_1^0$	26%
			$\to P_1 \tilde{\chi}_1^0$	0.4%
$\tilde{\chi}_4^0$	278.0	1.5	$\tilde{\chi}_4^0 \to Z \tilde{\chi}_1^0$	11%
			$\to Z \tilde{\chi}_2^0$	22%
			$\to Z \tilde{\chi}_3^0$	1%
			$\to W^\pm \tilde{\chi}_1^\mp$	43%
			$\to S_1 \tilde{\chi}_1^0$	7%
			$\to S_1 \tilde{\chi}_2^0$	0.2%
			$\to S_2 \tilde{\chi}_1^0$	8%
			$\to P_1 \tilde{\chi}_1^0$	7%
			$\to P_1 \tilde{\chi}_2^0$	0.7%
$\tilde{\chi}_5^0$	324.4	2.1	$\tilde{\chi}_5^0 \to Z \tilde{\chi}_1^0$	30%
			$\to Z \tilde{\chi}_2^0$	1.5%
			$\to Z \tilde{\chi}_3^0$	0.15%
			$\to W^\pm \tilde{\chi}_1^\mp$	57%
			$\to S_1 \tilde{\chi}_1^0$	0.01%
			$\to S_1 \tilde{\chi}_2^0$	0.02%
			$\to S_1 \tilde{\chi}_3^0$	5%
			$\to S_2 \tilde{\chi}_1^0$	1%
			$\to S_2 \tilde{\chi}_2^0$	4%
			$\to P_1 \tilde{\chi}_1^0$	0.4%
			$\to P_1 \tilde{\chi}_2^0$	0.7%
			$\to P_1 \tilde{\chi}_3^0$	0.06%
$\tilde{\chi}_1^\pm$	165.0	0.136	$\tilde{\chi}_1^+ \to W^+ \tilde{\chi}_1^0$	100%
$\tilde{\chi}_2^\pm$	319.5	2.0	$\tilde{\chi}_2^+ \to W^+ \tilde{\chi}_1^0$	32%
			$\to W^+ \tilde{\chi}_2^0$	1%
			$\to W^+ \tilde{\chi}_3^0$	34%
			$\to Z \tilde{\chi}_1^+$	29%
			$\to S_1 \tilde{\chi}_1^+$	5%
			$\to P_1 \tilde{\chi}_1^+$	0.3%

Table 3: Masses, widths and main branching ratios of the neutralino and chargino states at Born level for the reference point A (table 2).

3. Collider measurements in the nMSSM

The nMSSM can play a crucial role in baryogenesis and dark matter generation, depending on the parameters of the Higgs, chargino and neutralino sectors. In this section it is studied how the relevant particles can be discovered and the relevant parameters be determined at

Sparticle	Mass m [GeV]	Width Γ [GeV]	Decay modes	
S_1	115.2	0.044	$S_1 \to b\bar{b}$	8%
			$\to \tilde{\chi}_1^0 \tilde{\chi}_1^0$	92%
S_2	156.6	0.060	$S_2 \to b\bar{b}$	2%
			$\to W^+ W^-$	17%
			$\to ZZ$	2.5%
			$\to \tilde{\chi}_1^0 \tilde{\chi}_1^0$	69%
			$\to \tilde{\chi}_1^0 \tilde{\chi}_2^0$	10%
P_1	133.7	0.008	$P_1 \to \tilde{\chi}_1^0 \tilde{\chi}_1^0$	100%

Table 4: Masses, widths and main branching ratios of the light Higgs states, including one-loop top-stop corrections, for the reference point A (table 2).

future colliders.

3.1 The nMSSM at LHC

3.1.1 Higgs physics

In the benchmark scenario A, the light Higgs states S_1, S_2 and P_1 mainly decay invisibly into the lightest neutralinos. This behavior is rather typical for many singlet-extended supersymmetry models [40]. A CP-even invisible Higgs boson can be discovered at the LHC through W-boson fusion [41] and through associated Zh production [42]. The cross-sections and final state distributions for these processes in the nMSSM are the same as for the Standard Model Higgs boson, except for modified Higgs-Z couplings, that are given by

$$G_{\mathrm{ZZS_i}} = G_{\mathrm{ZZH}}^{\mathrm{SM}}(s_\beta O_{i1}^S + c_\beta O_{i2}^S). \tag{3.1}$$

For the reference point A (table 2), the couplings for the three CP-even Higgs states amount to

$$\begin{aligned}
G_{\mathrm{ZZS_1}} &= 0.87 \times G_{\mathrm{ZZH}}^{\mathrm{SM}}, \\
G_{\mathrm{ZZS_2}} &= 0.49 \times G_{\mathrm{ZZH}}^{\mathrm{SM}}, \\
G_{\mathrm{ZZS_3}} &= 0.002 \times G_{\mathrm{ZZH}}^{\mathrm{SM}}.
\end{aligned} \tag{3.2}$$

Since both the S_1 and S_2 states have $\mathcal{O}(1)$ couplings to the Z boson and are relatively light, with masses below $200\,\mathrm{GeV}$, they can be produced with sizable rates. Based on the analysis of ref. [41], it can be estimated that with only a few fb^{-1} of integrated luminosity, a 5σ discovery in the W-boson fusion channel can be achieved in the scenario A.

For the case of a single Standard-Model-like Higgs boson, the mass of the Higgs can be determined from the ratio of the W-boson fusion and Zh production rates [43]. On the other hand, in scenario A, the invisible Higgs signal receives contributions from both the S_1 and S_2. However, the observables in both W-boson fusion and Zh production are not sensitive to discriminate between one and two invisible Higgs states. As a result, from an invisible Higgs signal at the LHC, it is not possible to obtain information about the number and the masses of the CP-even Higgs bosons in the nMSSM.

Sparticle	Mass m [GeV]	Width Γ [GeV]	Decay modes	
$\tilde{t}_1$	522.1	43.1	$\tilde{t}_1 \to t\tilde{\chi}_1^0$	12%
			$\to t\tilde{\chi}_2^0$	7%
			$\to t\tilde{\chi}_3^0$	11%
			$\to t\tilde{\chi}_4^0$	20%
			$\to t\tilde{\chi}_5^0$	1%
			$\to b\tilde{\chi}_1^+$	47%
			$\to b\tilde{\chi}_2^+$	2%
$\tilde{t}_2$	535.3	29.8	$\tilde{t}_2 \to t\tilde{\chi}_1^0$	14%
			$\to t\tilde{\chi}_2^0$	2%
			$\to t\tilde{\chi}_3^0$	11%
			$\to t\tilde{\chi}_4^0$	9%
			$\to t\tilde{\chi}_5^0$	20%
			$\to b\tilde{\chi}_1^+$	6%
			$\to b\tilde{\chi}_2^+$	37%
$\tilde{b}_1$	498.8	6.6	$\tilde{b}_1 \to b\tilde{\chi}_1^0$	0.5%
			$\to b\tilde{\chi}_2^0$	12%
			$\to b\tilde{\chi}_3^0$	12%
			$\to b\tilde{\chi}_4^0$	0.1%
			$\to b\tilde{\chi}_5^0$	5%
			$\to t\tilde{\chi}_1^-$	57%
			$\to t\tilde{\chi}_2^-$	15%
$\tilde{b}_2$	503.3	12.5	$\tilde{b}_2 \to b\tilde{\chi}_1^0$	0.6%
			$\to b\tilde{\chi}_2^0$	4%
			$\to b\tilde{\chi}_3^0$	9%
			$\to b\tilde{\chi}_4^0$	0.2%
			$\to b\tilde{\chi}_5^0$	7%
			$\to t\tilde{\chi}_1^-$	56%
			$\to t\tilde{\chi}_2^-$	23%
$\tilde{g}$	730	6.6	$\tilde{g} \to b\tilde{b}_1$	35%
			$\to b\tilde{b}_2$	34%
			$\to t\tilde{t}_1$	18%
			$\to t\tilde{t}_2$	13%

Table 5: Masses, widths and main branching ratios of the third generation squarks and the gluino at Born level for the reference point A (table 2).

3.1.2 Supersymmetric particles

Since the partners of quarks and the gluon, squarks and gluino, couple with the strong QCD coupling, they are produced with large cross-sections at the LHC. Charginos and neutralino can be generated in the decay cascades of squarks and the gluino with sizeable rates. In principle, charginos and neutralino are also produced directly in electroweak processes, but

$pp \to$	$\tilde{g}\tilde{g}$	$\tilde{b}_1\tilde{b}_1^*$	$\tilde{b}_1\tilde{b}_2^*/\tilde{b}_2\tilde{b}_1^*$	$\tilde{b}_2\tilde{b}_2^*$	$\tilde{t}_1\tilde{t}_1^*$	$\tilde{t}_1\tilde{t}_2^*/\tilde{t}_2\tilde{t}_1^*$	$\tilde{t}_2\tilde{t}_2^*$	$\tilde{g}\tilde{b}_1^{(*)}$	$\tilde{g}\tilde{b}_2^{(*)}$
σ [fb]	2162	444	3	421	357	1	312	141	138

Table 6: Tree-level production cross-sections for strongly interacting supersymmetric particles at the LHC for the reference point A, see table 2. The QCD scale is taken at the average mass of the produced particles, $Q = (m_{\tilde{x}} + m_{\tilde{y}})/2$.

the cross-sections for these channels are small. Therefore in the following only squarks and gluinos are considered as primary supersymmetric particles. At the Tevatron, the typically large slepton masses necessary to suppress the electron electric dipole moment in this model lead to a reduced branching ratio for the decay of neutralinos and charginos into lepton final states. This makes their searches in the tri-lepton channel quite difficult, particularly for masses of the chargino and second lightest neutralino larger than 150 GeV, as are typical in the nMSSM scenario under analysis [44].

The relevant leading-order production cross-sections for squarks and gluinos at the LHC are summarized in table 6, calculated with COMPHEP 4.4 [45]. The analysis of $\tilde{\chi}_2^0$ production is experimentally particularly promising [46]. The neutralino $\tilde{\chi}_2^0$ is produced in various squark and gluino decay cascades, leading to a total cross-section for $\tilde{\chi}_2^0$ production with leptonic $\tilde{\chi}_2^0$ decays of 30 fb. Here the most important channel is

$$pp \to \tilde{g}\tilde{g}, \qquad \tilde{g} \to b\tilde{b}^* \text{ or } \bar{b}\tilde{b} \to b\bar{b}\tilde{\chi}_2^0, \tag{3.3}$$

but direct production of sbottoms and stops via $pp \to \tilde{b}\tilde{b}^*, \tilde{t}\tilde{t}^*$ also plays a role. According to ref. [47, 46], background from SM gauge bosons can be reduced by cuts on missing transverse energy and missing mass:

- At least three jets with transverse momentum $p_t^{\text{jet}} > 150, 100, 50$ GeV.

- Missing energy $\not{E} > \max(100 \text{ GeV}, 0.2 M_{\text{eff}})$ with $M_{\text{eff}} \equiv \not{E} + \sum_{i=1}^{3} p_{t,i}^{\text{jet}}$.

- Two isolated leptons with $p_t^{\text{lep}} > 20, 10$ GeV.

The remaining $t\bar{t}$ background is removed by subtracting events with two different-flavor leptons from events with same-flavor leptons. This procedure makes use of the fact that the $t\bar{t}$ background produces the same number of same-flavor and different-flavor lepton pairs, while the neutralino signal has only same-flavor lepton pairs. After these cuts practically no SM background is left, while a signal efficiency for $\tilde{\chi}_2^0$ production of better than 20% is achieved [47, 46]. This corresponds to about 1800 signal events for an integrated luminosity of 300 fb^{-1}.

The two-lepton signal for $\tilde{\chi}_2^0$ production can also originate from the neutralino $\tilde{\chi}_3^0$, whereas the contamination from heavier neutralinos is very small. The total cross-section for leptonic $\tilde{\chi}_3^0$ decays is 40 fb. Contrary to the $\tilde{\chi}_2^0$, the two leptons from $\tilde{\chi}_3^0$ originate from a real Z-boson and have an invariant mass equal to M_{Z}.

For the scenario A, see table 2, the production of neutralinos $\tilde{\chi}_2^0$ and $\tilde{\chi}_3^0$ has been simulated with COMPHEP 4.4 [45], using CTEQ6M parton distribution functions. The
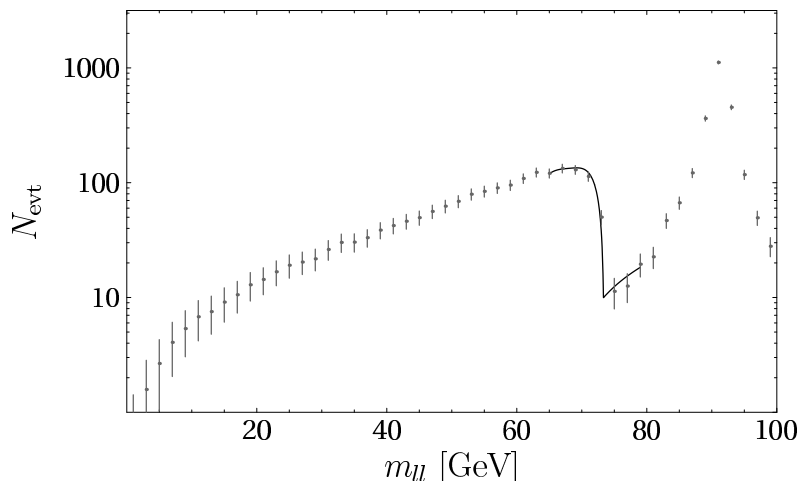
Figure 1: Fit to m_{ll} distribution for light neutralino production at the LHC. Backgrounds from Standard Model sources are not included, as they are expected to be small.

production cross-section is substantially modified by QCD corrections [48]. However, for the determination of superpartner masses, only the kinematic properties of the decay products are important, which are modified relatively little by radiative corrections. For the purpose of this work, radiative corrections have thus been neglected. Information about superpartner masses can be extracted from kinematic edges in invariant mass spectra of the final state particles [46, 49]. The distribution of the di-lepton invariant mass m_{ll} in $\tilde{\chi}_2^0$ decay has a sharp upper edge

$$m_{ll,\max,2} = m_{\tilde{\chi}_2^0} - m_{\tilde{\chi}_1^0}, \tag{3.4}$$

see figure 1. The peak at $m_{ll} = M_Z$ comes from the contribution of $\tilde{\chi}_3^0$, while events at lower invariant masses originate mainly from the $\tilde{\chi}_2^0$. Assuming $300\,\mathrm{fb}^{-1}$ luminosity, a simple fit to the upper edge of that region gives

$$m_{ll,\max,2} = 73.5 \pm 0.5 \pm 0.08 \text{ GeV}, \tag{3.5}$$

where the first error is statistical, while the second error accounts for the systematic error from energy scale uncertainty in the detector (see [47] for discussion). The error is comparable to what was found in [47] for the MSSM scenario (β).

For further studies, the decay chains involving the $\tilde{\chi}_3^0$ can be separated from the $\tilde{\chi}_2^0$ by applying the cut $|m_{ll} - M_Z| < 10\,\mathrm{GeV}$ on the di-lepton invariant mass. Including the jet from the squark decay $\tilde{b} \to b\tilde{\chi}_i^0$ gives additional information. For the decay chain with the $\tilde{\chi}_3^0$, the invariant $m_{jll,3}$ distribution has an upper endpoint with

$$m_{jll,\max,3}^2 = \frac{1}{2m_{\tilde{\chi}_3^0}^2}\Big[m_{\tilde{\chi}_1^0}^2 m_{\tilde{\chi}_3^0}^2 - m_{\tilde{\chi}_3^0}^4 - m_{\tilde{\chi}_1^0}^2 m_{\tilde{b}}^2 + m_{\tilde{\chi}_3^0}^2 m_{\tilde{b}}^2 + m_{\tilde{\chi}_3^0}^2 M_Z^2 + m_{\tilde{b}}^2 M_Z^2 \\ - (m_{\tilde{\chi}_3^0}^2 - m_{\tilde{b}}^2)\sqrt{\lambda(m_{\tilde{\chi}_1^0}^2, m_{\tilde{\chi}_3^0}^2, M_Z^2)} \Big]. \tag{3.6}$$

with $\lambda(a,b,c) = a^2 + b^2 + c^2 - 2ab - 2ac - 2bc$. Since the mass difference between $m_{\tilde{b}_1}$ and $m_{\tilde{b}_2}$ is small, no experimental distinction between the two states can and needs to be
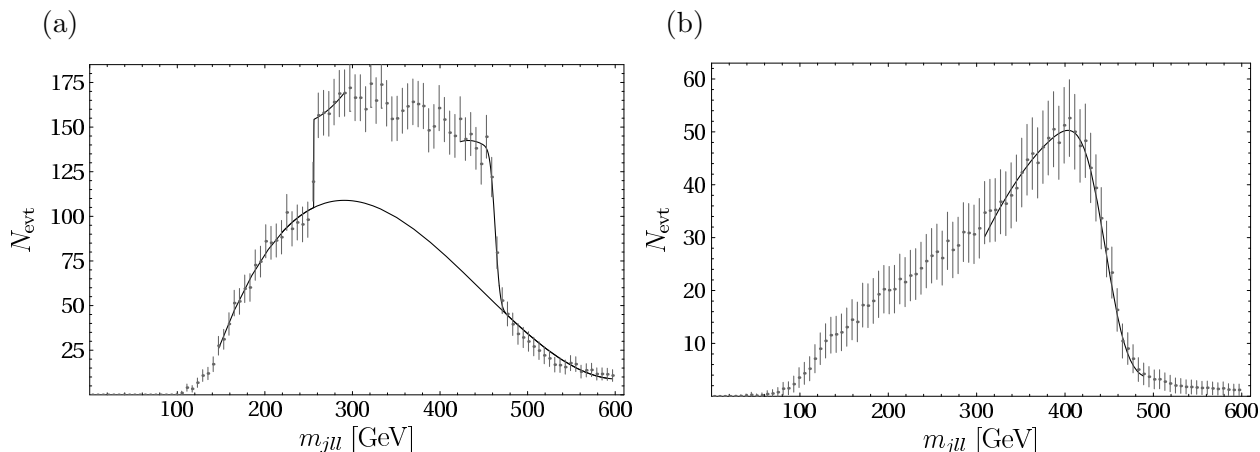
Figure 2: Fits to the m_{jll} distribution for (a) $\tilde{\chi}_3^0$ and (b) $\tilde{\chi}_2^0$ production at the LHC. Backgrounds from Standard Model sources are not included, as they are expected to be small.

made. Flavor-tagging of the b-jet from the sbottom decay does not improve the analysis, since the main background is $t\bar{t}$.

In a typical supersymmetry event, there are multiple jets. The jet from $\tilde{b} \to b\tilde{\chi}_i^0$ is expected to be relatively hard $E_{\mathrm{T,j}} \gtrsim 200\,\mathrm{GeV}$, but there are additional hard jets from the decay of the other sbottom and from gluinos, $\tilde{g} \to b\tilde{b}$. This introduces an irreducible combinatorial background. However, including that background, the characteristic edge in the $m_{jll,3}$ distribution at $m_{jll,\mathrm{max},3}$ is still visible, see figure 2. The combinatorial background can be reduced by special techniques [47, 46], but here we simply choose to fit it. The fit result is

$$m_{jll,\mathrm{max},3} = 463.6^{+5.5}_{-9.0} \pm 2.3 \text{ GeV}, \tag{3.7}$$

where as before the second error includes lepton and jet energy scale uncertainties. A second edge in the $m_{jll,3}$ distribution is found at

$$m_{jll,\mathrm{min},3}^2 = \frac{1}{2m_{\tilde{\chi}_3^0}^2}\Big[m_{\tilde{\chi}_1^0}^2 m_{\tilde{\chi}_3^0}^2 - m_{\tilde{\chi}_3^0}^4 - m_{\tilde{\chi}_1^0}^2 m_{\tilde{b}}^2 + m_{\tilde{\chi}_3^0}^2 m_{\tilde{b}}^2 + m_{\tilde{\chi}_3^0}^2 M_Z^2 + m_{\tilde{b}}^2 M_Z^2 $$
$$+ (m_{\tilde{\chi}_3^0}^2 - m_{\tilde{b}}^2)\sqrt{\lambda(m_{\tilde{\chi}_1^0}^2, m_{\tilde{\chi}_3^0}^2, M_Z^2)}\Big], \tag{3.8}$$

which can be fitted in the same way as the upper end point, yielding

$$m_{jll,\mathrm{min},3} = 256.2^{+6.0}_{-7.0} \pm 1.3 \text{ GeV}. \tag{3.9}$$

In addition to studying the decay chain with the $\tilde{\chi}_3^0$, by requiring the invariant mass of the lepton pair to be sufficiently below the Z pole, $m_{ll} < M_Z - 10$ GeV, the decay chain with the $\tilde{\chi}_2^0$ can be selected. Similarly to the $\tilde{\chi}_3^0$ case, the $m_{jll,\mathrm{max},2}$ distribution has a characteristic endpoint at

$$m_{jll,\mathrm{max},2}^2 = \frac{1}{m_{\tilde{\chi}_2^0}^2}(m_{\tilde{\chi}_2^0}^2 - m_{\tilde{\chi}_1^0}^2)(m_{\tilde{b}}^2 - m_{\tilde{\chi}_2^0}^2). \tag{3.10}$$

– 16 –

As the $\tilde{\chi}_2^0$ decays through an off-shell Z^*, the $m_{jll,\mathrm{max},2}$ distribution has no characteristic endpoint towards the lower end. To first approximation, the spectrum of $\tilde{\chi}_2^0$ decays via an off-shell Z^* can be thought of as superposition of Breit-Wigner line-shapes, which are close to Gaussian. Consequently, the upper end of the $m_{jll,\mathrm{max},2}$ distribution can be approximated by an error function. A fit gives the rather poor result

$$m_{jll,\mathrm{max},2} = 447^{+14}_{-21} \pm 2.3 \text{ GeV}, \tag{3.11}$$

which is limited by statistics and the shape of the distribution near the endpoint, which is less steep than for the di-lepton distribution.

Light charginos $\tilde{\chi}_1^\pm$ can be detected in the squark decay chains by looking for a same-sign lepton signal originating from the processes

$$
\begin{aligned}
pp \to \tilde{g}\tilde{g} &\to b\tilde{b}^*\tilde{b}^* \to bb\,\overline{tt}\,\tilde{\chi}_1^+\tilde{\chi}_1^+ \to bb\,\overline{tt}\,W^+W^+\,\tilde{\chi}_1^0\tilde{\chi}_1^0 \to bb\,\overline{tt}\,l^+l^+\,\nu_l\nu_l\,\tilde{\chi}_1^0\tilde{\chi}_1^0,\\
pp \to \tilde{g}\tilde{g} &\to \overline{bb}\,\tilde{b}\tilde{b} \to \overline{bb}\,tt\,\tilde{\chi}_1^-\tilde{\chi}_1^- \to \overline{bb}\,tt\,W^-W^-\,\tilde{\chi}_1^0\tilde{\chi}_1^0 \to \overline{bb}\,tt\,l^-l^-\,\bar{\nu}_l\bar{\nu}_l\,\tilde{\chi}_1^0\tilde{\chi}_1^0,\\
pp \to \tilde{g}\tilde{g} &\to tt\tilde{t}^*\tilde{t}^* \to tt\,\overline{bb}\,\tilde{\chi}_1^-\tilde{\chi}_1^- \to tt\,\overline{bb}\,W^-W^-\,\tilde{\chi}_1^0\tilde{\chi}_1^0 \to tt\,\overline{bb}\,l^-l^-\,\bar{\nu}_l\bar{\nu}_l\,\tilde{\chi}_1^0\tilde{\chi}_1^0,\\
pp \to \tilde{g}\tilde{g} &\to \overline{tt}\,\tilde{t}\tilde{t} \to \overline{tt}\,bb\,\tilde{\chi}_1^+\tilde{\chi}_1^+ \to \overline{tt}\,bb\,W^+W^+\,\tilde{\chi}_1^0\tilde{\chi}_1^0 \to \overline{tt}\,bb\,l^+l^+\,\nu_l\nu_l\,\tilde{\chi}_1^0\tilde{\chi}_1^0,
\end{aligned}
\tag{3.12}
$$

see ref. [50]. However, since besides the neutralino as the lightest supersymmetric particle, the neutrino in the chargino decay also escapes detection, the remaining lepton-jet invariant mass distributions do not allow a meaningful mass extraction.

The measurement of the heavy neutralinos $\tilde{\chi}_4^0$ and $\tilde{\chi}_5^0$ at the LHC is very difficult. As pointed out above, the appearance of a lepton pair in the neutralino decay is the best possibility for detection. However, due to small branching ratios of the heavy neutralinos into leptons, the statistics for this channel are very low.

From the combination of the results in eqs. (3.5), (3.7), (3.9), and (3.11) one can extract the following absolute values for the superpartner masses,

$$m_{\tilde{\chi}_1^0} = 33^{+32}_{-17.5} \text{ GeV}, \quad m_{\tilde{\chi}_2^0} = 106.5^{+32.5}_{-17.5} \text{ GeV}, \quad m_{\tilde{\chi}_3^0} = 181^{+20}_{-10} \text{ GeV}, \quad m_{\tilde{b}} = 499^{+30}_{-17} \text{ GeV}. \tag{3.13}$$

The large errors are due to large correlations between the mass parameters, as illustrated for one example in figure 3. This can be explained by the fact that all measurements of kinematic endpoints in the decay distributions are closely related to mass *differences*, whereas no independent direct measurement of one of the masses, e.g. the lightest neutralino mass, is available.

The analysis in this section has been performed for the specific parameter point A (see table 2). However, most of the results are expected to be rather typical for nMSSM scenarios that explain baryogenesis and dark matter. These two constraints predict that all neutralino and chargino states should be relatively light. In addition, our LHC analysis relies heavily on the gluino and a sbottom state with large left-chiral component to have masses of the order of a few hundred GeV. At present, the mass of the gluino is not constrained by any data, but if GUT-scale gaugino unification is realized, the gluino should have a mass of about 1 TeV or less. As discussed before, the presence of light squarks
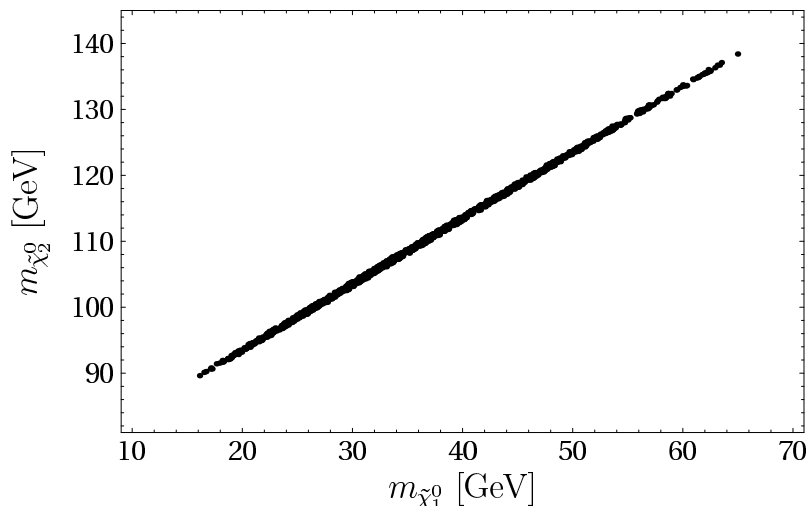
Figure 3: Correlation between $m_{\tilde{\chi}_1^0}$ and $m_{\tilde{\chi}_2^0}$ from LHC measurements.

are helpful in avoiding the suppression of chiral charges leading to the generation of the baryon asymmetry in this model. Following ref. [16] we have therefore assumed that the third generation squarks have masses of the order of $500\,\mathrm{GeV}$. While, as emphasized above, this assumption is crucial in the analysis of the LHC phenomenology, it plays only a minor role in the ILC related one. At an e^+e^- collider such as the ILC, a precise measurement of the lightest neutralino mass is possible, so that by combing results from the LHC and ILC, the precision of the neutralino mass determination can be greatly improved. This was discussed already for the MSSM in ref. [46] and will be analyzed for the nMSSM in the next sections.

3.2 The nMSSM at Giga-Z

In nMSSM scenarios that account for baryogenesis and cold dark matter, the lightest neutralino mass is typically smaller than half the Z-boson mass, $m_{\tilde{\chi}_1^0} < M_\mathrm{Z}/2$. In particular this is the case in the reference point A (cf. table 3). As a consequence, the lightest neutralino contributes to the invisible Z width. Current limits from LEP [51] already pose strong constraints on the nMSSM parameter space [25]. Nevertheless, these constraints can be improved at a future high-luminosity linear collider (ILC) running on the Z pole [52]. This "Giga-Z" option for the ILC could collect $50\,\mathrm{fb}^{-1}$ of integrated luminosity at $\sqrt{s} \sim M_\mathrm{Z}$, which is an improvement of several orders of magnitude compared to LEP.

Since in a typical scenario like reference point A, the neutralino dark matter annihilation proceeds almost exclusively via s-channel Z-exchange, the precise determination of the invisible Z width opens up the opportunity to directly and model-independently determine the relevant $Z\tilde{\chi}_1^0\tilde{\chi}_1^0$ coupling

$$|G_{Z\tilde{\chi}_1^0\tilde{\chi}_1^0}|^2 = \frac{g^2}{4c_\mathrm{W}^2}\left(|N_{13}|^2 - |N_{14}|^2\right)^2. \tag{3.14}$$

However, the achievable accuracy at Giga-Z for $\Gamma_\mathrm{inv}^\mathrm{Z}$ is limited by systematics, and can reach at best 0.1% [53], which is only a factor 4 better than current LEP constraints. This

corresponds to an error of about 0.2×10^{-3} for $\text{BR}[Z \to \tilde{\chi}_1^0 \tilde{\chi}_1^0]$. In the case of scenario A, $\text{BR}[Z \to \tilde{\chi}_1^0 \tilde{\chi}_1^0] \approx 0.3 \times 10^{-3}$, so that the dark matter relic density can be determined from the invisible Z width with an uncertainty of at best 60%. Here it is assumed that the mass $m_{\tilde{\chi}_1^0}$ is determined from some other observable with a much smaller error.

Despite the large error, a Giga-Z analysis can confirm the existence of a neutral, (quasi-)stable, weakly interacting particle and a rough estimate of its coupling to the Z boson in a model-independent way. This would also be an interesting cross-check for more detailed model-dependent measurements at higher energies.

3.3 The nMSSM at ILC

3.3.1 Higgs physics

The CP-even Higgs bosons can be produced in e^+e^- collisions through radiation off a Z boson, $e^+e^- \to S_i Z$. This process is very similar to the case of the Standard Model Higgs boson, except for the different Higgs-Z couplings strength as in eq. (3.1). The S_1 and S_2 states have relatively large couplings to the Z boson, see eq. (3.2), and are therefore produced in sizeable rates.

As mentioned above, both S_1 and S_2 decay predominantly invisibly into the lightest neutralino in scenario A. Nevertheless, the kinematic mass peaks of the Higgs bosons can be reconstructed from the recoil of the Z, which is cleanly characterized by the leptonic Z decays $Z \to e^+e^-$ and $Z \to \mu^+\mu^-$ [54, 55]. Due to photon radiation and detector resolution effects, the reconstructed mass peaks are smeared out somewhat, but their width is less than $10\,\text{GeV}$, so that the two states S_1 and S_2 can be clearly distinguished.

Taking into account the reduced G_{ZZS_i} couplings with respect to the SM, the Higgs masses can be determined from the Z recoil spectrum with the precision [54]

$$\delta M_{S1} \approx 130 \text{ MeV}, \qquad \delta M_{S2} \approx 185 \text{ MeV}. \tag{3.15}$$

Based on similar studies for the SM-like and invisible Higgses [56, 55], the branching ratios of S_1 and S_2 can be extracted with the following accuracy,

$$BR[S_1 \to b\bar{b}] = (8 \pm 0.7)\%, \qquad BR[S_1 \to \text{inv.}] = (91 \pm 3)\%,$$
$$BR[S_2 \to b\bar{b}] = (2 \pm 0.3)\%, \qquad BR[S_2 \to \text{inv.}] = (79 \pm 5)\%, \tag{3.16}$$
$$BR[S_2 \to W^+W^-] = (17 \pm 1.5)\%.$$

Here only the statistical error is given, taking into account selection cuts to reduce the backgrounds. The large invisible branching ratio of both scalar states points towards a sizeable Higgs self-coupling λ.

The light pseudo-scalar P_1 is an almost pure singlet, and the production cross-section $e^+e^- \to S_i P_1$ suppressed by more than two orders of magnitude with respect to the corresponding process in the MSSM. Furthermore, the only available final state $b\bar{b} + \not{E}$ is swamped by background from $S_i Z$ production, so that it appears impossible to discover the P_1 at the ILC.

The two heavy neutral Higgs bosons S_3 and P_2 as well as the charged Higgs boson are too heavy be produced at the ILC with center-of-mass energies up to $1\,\text{TeV}$. In particular the charged Higgs boson should always have a clearly visible decay channel into top-

$e^+e^- \to \tilde\chi_i^0 \tilde\chi_j^0$	$\tilde\chi_i^0 = \tilde\chi_2^0$	$\tilde\chi_3^0$	$\tilde\chi_4^0$	$\tilde\chi_5^0$
$\tilde\chi_j^0 = \tilde\chi_1^0$	2.0	5.4	3.7	3.9
$\tilde\chi_2^0$	0.4	0.6	16.2	0.1
$\tilde\chi_3^0$		0.1	32.8	—
$\tilde\chi_4^0$			—	—
$\tilde\chi_5^0$				—
$e^+e^- \to \tilde\chi_i^\pm \tilde\chi_j^\mp$	$\tilde\chi_i^\pm = \tilde\chi_1^\pm$	$\tilde\chi_2^\pm$		
$\tilde\chi_j^\mp = \tilde\chi_1^\mp$	594	32.2		
$\tilde\chi_2^\mp$		—		

Table 7: Tree-level production cross-sections in fb at $\sqrt{s} = 500\,\text{GeV}$ with unpolarized beams for the reference point A (table 2).

and bottom-quarks, $H^+ \to t\bar{b}$. Charged Higgs production proceeds mainly through an s-channel photon (with only a sub-dominant contribution from s-channel Z exchange) and thus cannot be suppressed by modified couplings. As a consequence, the non-observation of the charged Higgs would clearly indicate that M_A is large, $M_A > \sqrt{s}/2$. In this case, from the observation of the two light invisibly decaying Higgs states, it can be deduced that these two Higgs bosons must be mixtures of the SM-like Higgs and a new singlet. In other words, from the analysis of the Higgs bosons at the 500 GeV ILC, one can already identify an extended Higgs sector beyond the two doublets in the MSSM.

3.3.2 Supersymmetric particles

In scenario A, many of the neutralino and chargino states are produced with sizeable cross-sections at the ILC with $\sqrt{s} = 500\,\text{GeV}$, as shown in table 7. The most promising production processes are $e^+e^- \to \tilde\chi_2^0\tilde\chi_4^0$, $\tilde\chi_3^0\tilde\chi_4^0$, $\tilde\chi_1^+\tilde\chi_1^-$, $\tilde\chi_1^\pm\tilde\chi_2^\mp$, with cross-sections of more than 10 fb each. While the lightest neutralino is not produced directly with large rates, it can nevertheless be studied in great detail in the decays of the heavier neutralinos and charginos.

In the following subsections, the most promising decay channels will be analyzed in detail, including Standard Model and supersymmetric backgrounds. It is found that the two charginos and all neutralinos except the $\tilde\chi_5^0$ could be discovered and their masses and cross-sections measured. The discovery of a fifth neutralino state would be a smoking gun for a non-minimal supersymmetric model, but turns out to be very challenging experimentally. Nevertheless, the discovery of two neutralino states which are much lighter than the lightest chargino is already clear evidence for physics beyond the MSSM, where only one neutralino, a dominant bino-state, can be significantly lighter than the charginos.

We simulated signal and background with the Monte-Carlo methods from [57], including full tree-level matrix elements and Breit-Wigner parameterizations for resonant intermediate particles. Initial-state radiation and beamstrahlung are always included. The processes are generated at the parton level, but jet energy fluctuations through parton shower and detector effects are parameterized by smearing functions with lep-

$P(e^+)/P(e^-)$	$\tilde{\chi}_2^0\tilde{\chi}_4^0$	$\tilde{\chi}_3^0\tilde{\chi}_4^0$	$\tilde{\chi}_1^+\tilde{\chi}_1^-$	$\tilde{\chi}_1^\pm\tilde{\chi}_2^\mp$	W^+W^-	ZZ	$t\bar{t}$	W^+W^-Z
80% left / 50% right	25.8	52.2	1557	51.3	24500	1020	1130	95
80% right / 50% left	19.6	39.7	107	39.0	770	440	500	4.5

Table 8: Polarized tree-level production cross-sections in fb for neutralino, chargino and some of the largest SM background processes at $\sqrt{s} = 500\,\mathrm{GeV}$ for the reference point A (table 2).

ton and jet energy uncertainties taken from [58]. Jets overlapping within a cone with $\Delta R = \sqrt{(\phi_1 - \phi_2)^2 + (\eta_1 - \eta_2)^2} < 0.3$ are combined into one jet, where ϕ_i and η_i are the azimuthal angle and rapidity of jet i. Similarly, a lepton lying within a jet is combined into the jet. Leptons and jets outside the central region of the detector have a higher likelihood of mistag and get inflicted by the large two-photon background. Therefore leptons within an angle of $|\cos\theta| < 0.95$ around the beam line and jets with $|\cos\theta| < 0.90$ are discarded. After these simple procedures, the remaining isolated jets and leptons define the signature of the simulated event.

For most processes, the signal cross-sections can be enhanced and background can be reduced by a suitable choice of beam polarization. Here we assume that both the electron and positron beam are polarized, with polarization degrees of 80% and 50%, respectively. It is further assumed that $500\,\mathrm{fb}^{-1}$ of luminosity is spent for $P(e^+)/P(e^-) = \mathrm{left/right}$ and right/left each. The center-of-mass energy is always $\sqrt{s} = 500\,\mathrm{GeV}$. The signal and main SM background cross-sections for polarized beams are summarized in table 8.

For all neutralino and chargino processes under study here, the main SM background come from double and triple gauge boson production, $t\bar{t}$ production and two-photon processes. Quite generally, they can be reduced by observing that the supersymmetric signal processes lead to large missing energy, and most of the final state particles go in the central detector region. In particular, by imposing a minimum value for the total transverse momentum, $p_t > 12\,\mathrm{GeV}$, the two-photon background is practically completely removed[4] [7]. Furthermore, cuts on the missing energy $\not{E}$, the polar angle of the missing momentum, $\cos\theta_{p_{\mathrm{miss}}}$, and of the visible momentum, $\cos\theta_{p_{\mathrm{tot}}} = p_{\mathrm{long}}/p_{\mathrm{tot}}$ are effective to reduce the Standard Model backgrounds.

3.3.3 Chargino $\tilde{\chi}_1^+$

The lightest charginos almost exclusively decay via $\tilde{\chi}_1^\pm \to W^\pm \tilde{\chi}_1^0$, where the W can decay leptonically or hadronically. Since charginos are produced in pairs, two W bosons appear in their decays. If both W's decay leptonically, the rates are relatively low and one has

---

[4]Note that the rejection of the two-photon and $e^\pm$-γ background depends crucially on an excellent coverage of the detector at low polar angles, so that energetic fermions with low transverse momentum can be vetoed. The results of ref. [7] are based on the detector design of the TESLA study [58], with low beam crossing angle, muon detectors extending to 65 mrad, and endcap calorimeters extending to 27.5 mrad. Although for the current ILC detector R & D several changes in the details of this setup are discussed, the planned ILC detector designs are expected to reach a similar photon-induced background rejection [59]. However, we also want to point out that the simulation of the photon-induced background in ref. [7] with PYTHIA [60] has unquantified and possibly large theoretical uncertainties.

to deal with a difficult background from W^+W^-. The purely hadronic final state, on the other hand, is plagued by jet pair combination ambiguities. Therefore the best mode is: $e^+e^- \rightarrow \tilde{\chi}_1^+ \tilde{\chi}_1^- \rightarrow W^+W^- \tilde{\chi}_1^0 \tilde{\chi}_1^0 \rightarrow jj\, l^\pm + \not{E}$ where j stands for a jet. The most important SM backgrounds are W^+W^-, ZZ, $t\bar{t}$ and two-photon production, while supersymmetric backgrounds from neutralino pairs, ZS_i and Higgs pairs are also taken into account.

The SM backgrounds can be reduced by the general cuts explained in the previous section, $p_t > 12\,\text{GeV}$, $\not{E} > 100\,\text{GeV}$ and $|\cos\theta_{p_{\text{miss}}}| < 0.8$. Since the two jets in the signal originate from a W boson, the invariant jet mass is required to fulfill $|m_{jj} - M_{\text{W}}| < 10\,\text{GeV}$, which removes neutralino background and is also effective on $t\bar{t}$. The WW and $t\bar{t}$ backgrounds are further reduced by placing a cut on the reconstructed invariant mass of lepton and missing momentum, $m_{l,\text{miss}} > 150\,\text{GeV}$.

Both the signal and the main background are increased for the beam polarization combination $P(e^+)/P(e^-) = \text{right/left}$, but since the signal cross-section is large, and backgrounds after cuts are relatively low, this polarization combination helps to increase the measurement precision.

With the selection cuts listed above, about $S = 105000$ signal events are retained while only $B = 30000$ background events survive (mainly from Standard Model sources). The statistical error for total cross-section measurement is $\delta\sigma_{11,\text{L}}^\pm = 0.35\%$. For the opposite polarization combination, $P(e^+)/P(e^-) = \text{left/right}$, we obtain $\delta\sigma_{11,\text{R}}^\pm = 1.3\%$.

The distribution of the W-boson energy from chargino decay, reconstructed from the momenta of the two jets, can be used for a chargino mass measurement. The energy spectrum of the W boson is almost evenly distributed with characteristic endpoints at

$$E_{\text{min,max}} = \frac{1}{4m_{\tilde{\chi}_1^\pm}^2}\left[(m_{\tilde{\chi}_1^\pm}^2 - m_{\tilde{\chi}_1^0}^2 + M_{\text{W}}^2)\sqrt{s} \mp \sqrt{\lambda(m_{\tilde{\chi}_1^\pm}^2, m_{\tilde{\chi}_1^0}^2, M_{\text{W}}^2)(s - 4m_{\tilde{\chi}_1^\pm}^2)}\right]. \quad (3.17)$$

The energy distribution edges can be fitted by using a step function which is convoluted with the initial-state radiation and beamstrahlung spectrum and with the jet smearing function. The fit function is fitted to the distribution obtained from the Monte-Carlo simulation with a binned χ^2 fit. The fit results are (see figure 4)

$$E_{\text{min}} = 83.73^{+0.025}_{-0.011}\text{ GeV} \qquad\qquad E_{\text{max}} = 214.8 \pm 0.8\text{ GeV}. \quad (3.18)$$

resulting in

$$m_{\tilde{\chi}_1^\pm} = 165.0 \pm 0.3\text{ GeV} \qquad\qquad m_{\tilde{\chi}_1^0} = 33.3^{+1.2}_{-1.1}\text{ GeV}. \quad (3.19)$$

Note that only the statistical error has been given here, while the analysis of systematic errors at this level of precision would require a more elaborate investigation. Experience from the W mass measurement at LEP however shows that the systematic errors can be controlled to better than this level of accuracy.

3.3.4 Threshold scan for chargino $\tilde{\chi}_1^\pm$

In the determination of the chargino and lightest neutralino masses from the decay distribution, the precision is limited due to substantial correlation between $m_{\tilde{\chi}_1^\pm}$ and $m_{\tilde{\chi}_1^0}$ in
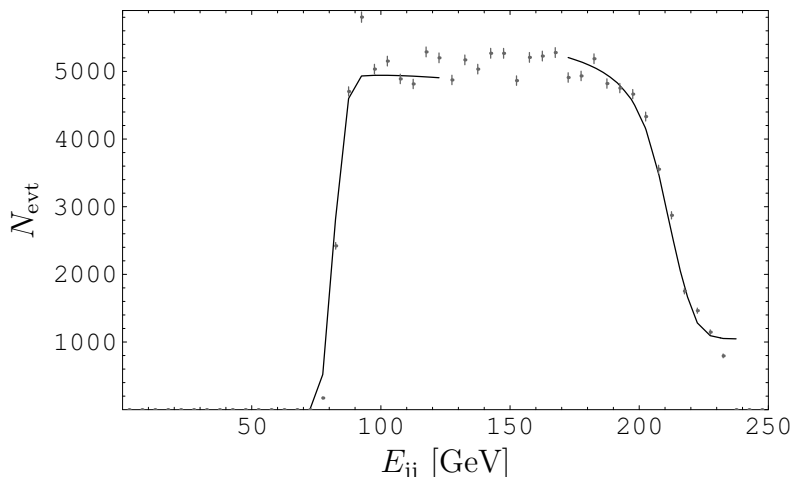
Figure 4: Energy distribution for the jet pair originating from the W boson in the decay $\tilde{\chi}_1^\pm \rightarrow W^\pm \tilde{\chi}_1^0$ after selection cuts, with a simple fit to the kinematic endpoints.

the analysis. This can be improved by using an independent measurement of $m_{\tilde{\chi}_1^\pm}$ via a threshold scan.

As an example, the measurement of the chargino pair production cross-section at six different center-of-mass energies below and above the nominal threshold $E_{\text{thr}} = 2m_{\tilde{\chi}_1^\pm} = 330$ GeV are considered. Here it is assumed that the chargino mass is already roughly known from distribution measurements studied above. The measurements below the threshold allow to determine the background and extrapolate to values $\sqrt{s} > 2m_{\tilde{\chi}_1^\pm}$, where the chargino excitation curve sets in. In combination with measurements above the threshold, the threshold energy E_{thr} can be precisely determined.

It is assumed that $10\,\text{fb}^{-1}$ luminosity is spent per point, amounting to total of $60\,\text{fb}^{-1}$. As before, the beams are polarized with $P(e^+)/P(e^-) = $ right/left, and the same selection cuts as in the previous subsection are applied. Since the chargino mass can already be determined from decay distributions, this information together with eq. (3.17) can be used to reduce the background further. The result of a simulation performed with this procedure is shown in figure 5. A fit with a simple quadratic function gives a very small statistical error,

$$E_{\text{thr}} = 329.97 \pm 0.1 \pm 0.03 \text{ GeV}, \tag{3.20}$$

where the second error comes from the uncertainty in the incoming beam energy, which is estimated to be of the order 10^{-4} [61]. This corresponds to $m_{\tilde{\chi}_1^\pm} = 164.98 \pm 0.05$ GeV. Together with the information from kinematic edges in eq. (3.18), the lightest neutralino mass is constrained to

$$m_{\tilde{\chi}_1^0} = 33.3^{+0.4}_{-0.3} \text{ GeV}. \tag{3.21}$$

3.3.5 Neutralino $\tilde{\chi}_3^0 \tilde{\chi}_4^0$

Both $\tilde{\chi}_3^0$ and $\tilde{\chi}_4^0$ have sizeable branching ratios into Z bosons, $\text{BR}[\tilde{\chi}_3^0 \rightarrow Z\tilde{\chi}_1^0] = 74\%$ and $\text{BR}[\tilde{\chi}_4^0 \rightarrow Z\tilde{\chi}_1^0] = 11\%$. This decay has the advantage of leading to very clear final state
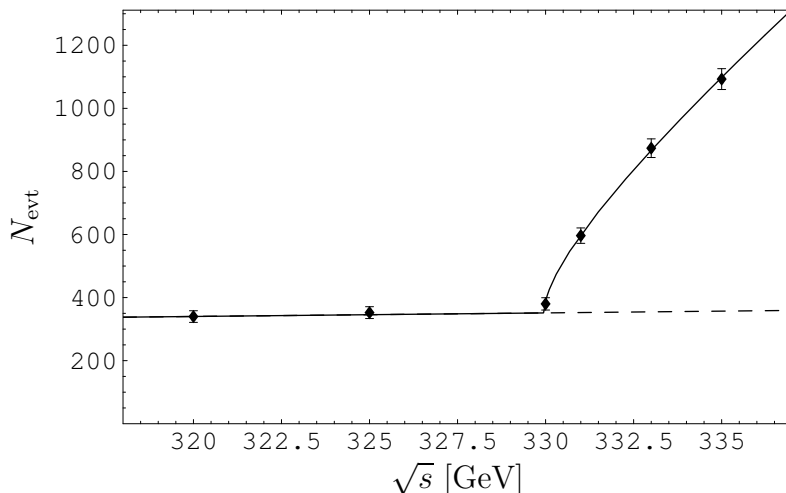
Figure 5: Threshold scan for chargino pair production at ILC.

signatures, and small background contamination from SM processes involving W-boson. Because of small branching ratio of the Z into leptons, only the hadronic final states are promising for the analysis of the neutralinos, at the cost of dealing with higher backgrounds and jet pair combination ambiguities. Then the signature is: $e^+e^- \to \tilde{\chi}_3^0\tilde{\chi}_4^0 \to ZZ\,\tilde{\chi}_1^0\,\tilde{\chi}_1^0 \to 4j + \not{E}$.

The largest SM backgrounds arise from ZZ, W^+W^-, $t\bar{t}$ and two-photon processes, but supersymmetric background from production of other neutralino pairs is also important, $e^+e^- \to \tilde{\chi}_i^0\tilde{\chi}_j^0$, with $(i,j) \neq (3,4)$. The SM backgrounds can be suppressed by choosing $P(e^+)/P(e^-) = \text{left/right}$, while the neutralino signal remains sizeable for this polarization combination. With the general cuts mentioned above, $p_t > 12\,\text{GeV}$, $\not{E} > 100\,\text{GeV}$ and $|p_{\text{long}}/p_{\text{tot}}| < 0.9$, the backgrounds are further reduced. In addition, two pairs of jets have to form the invariant Z mass, $|m_{j_1j_2} - M_Z| < 10\,\text{GeV}$ and $|m_{j_3j_4} - M_Z| < 10\,\text{GeV}$, which removes $\tilde{\chi}_2^0\tilde{\chi}_i^0$ background and is also effective on $t\bar{t}$. The $t\bar{t}$ background is reduced even further by using an anti-bottom-tag with efficiency 95% and a mistag rate of 3% for light flavors and 25% for charm jets [62].

After these cuts, $S = 400$ signal events and only $B = 38$ background events remain, leading to a statistical error for total cross-section measurement of $\delta\sigma_{34}^0 = 5.2\%$.

The energy spectrum of the Z-bosons from neutralino decay has characteristic upper and lower endpoints both for the $\tilde{\chi}_3^0$ and $\tilde{\chi}_4^0$, given by the expressions

$$
\begin{aligned}
E_{\text{min,max},3} = \frac{1}{4m_{\tilde{\chi}_3^0}^2\sqrt{s}} &\Big(m_{\tilde{\chi}_3^0}^4 - m_{\tilde{\chi}_3^0}^2 m_{\tilde{\chi}_4^0}^2 + m_{\tilde{\chi}_3^0}^2 M_Z^2 - m_{\tilde{\chi}_4^0}^2 M_Z^2 + m_{\tilde{\chi}_3^0}^2 s + M_Z^2 s \\
&- m_{\tilde{\chi}_1^0}^2(m_{\tilde{\chi}_3^0}^2 - m_{\tilde{\chi}_4^0}^2 + s) \mp \sqrt{\lambda(m_{\tilde{\chi}_3^0}^2, m_{\tilde{\chi}_1^0}^2, M_Z^2)\,\lambda(m_{\tilde{\chi}_3^0}^2, m_{\tilde{\chi}_4^0}^2, s)} \Big), \\
E_{\text{min,max},4} = \frac{1}{4m_{\tilde{\chi}_4^0}^2\sqrt{s}} &\Big(m_{\tilde{\chi}_4^0}^4 - m_{\tilde{\chi}_3^0}^2 m_{\tilde{\chi}_4^0}^2 + m_{\tilde{\chi}_4^0}^2 M_Z^2 - m_{\tilde{\chi}_3^0}^2 M_Z^2 + m_{\tilde{\chi}_4^0}^2 s + M_Z^2 s \\
&- m_{\tilde{\chi}_1^0}^2(m_{\tilde{\chi}_4^0}^2 - m_{\tilde{\chi}_3^0}^2 + s) \mp \sqrt{\lambda(m_{\tilde{\chi}_4^0}^2, m_{\tilde{\chi}_1^0}^2, M_Z^2)\,\lambda(m_{\tilde{\chi}_3^0}^2, m_{\tilde{\chi}_4^0}^2, s)} \Big),
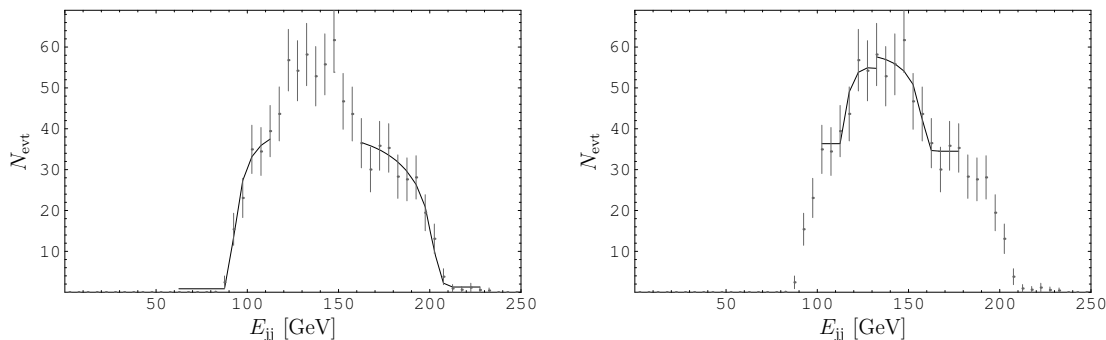\end{aligned}
$$

$$(3.22)$$

Figure 6: Energy distribution for the jet pair originating from Z bosons in the decays of the neutralinos for the process $e^+e^- \to \tilde{\chi}_3^0 \tilde{\chi}_4^0$. The plots show the expected event rates after selection cuts, with a simple fit to the kinematic edges.

Since we consider the same decay mode for the Z bosons stemming from both neutralinos, a distinction between the decay products of the $\tilde{\chi}_3^0$ and $\tilde{\chi}_4^0$ is not possible. Therefore, the measured spectrum contains all four kinematic edges at the same time, which can be fitted with a convoluted step function as above. From the fit, see figure 6, one obtains

$$ m_{\tilde{\chi}_3^0} = 181.5 \pm 7.6 \text{ GeV} \qquad\qquad m_{\tilde{\chi}_4^0} = 278.0 \pm 11.5 \text{ GeV}, \qquad (3.23) $$

while no good constraint on $m_{\tilde{\chi}_1^0}$ is obtained. The masses of both $\tilde{\chi}_3^0$ and $\tilde{\chi}_4^0$ can be determined, but due to the low statistics, the error is relatively large.

3.3.6 Neutralino $\tilde{\chi}_2^0 \tilde{\chi}_4^0$

The analysis of $\tilde{\chi}_2^0 \tilde{\chi}_4^0$ production works similarly to the $\tilde{\chi}_3^0 \tilde{\chi}_4^0$ production described in the previous subsection. The main difference lies in the fact that the $\tilde{\chi}_2^0$, due to small mass difference to the lightest neutralino $\tilde{\chi}_1^0$, decays only through a virtual, not on-shell, Z boson. Again, the best statistical significance of the signal is achieved by focusing on the hadronic decay modes of the Z bosons, $e^+e^- \to \tilde{\chi}_2^0 \tilde{\chi}_4^0 \to ZZ^* \tilde{\chi}_1^0 \tilde{\chi}_1^0 \to 4j + \not{\!\!E}$, and choosing the polarization combination $P(e^+)/P(e^-) = \text{left/right}$.

The backgrounds from ZZ, W^+W^-, $t\bar{t}$ and two-photon processes as well as $\tilde{\chi}_3^0 \tilde{\chi}_4^0$ neutralino production can be further reduced by the usual selection cuts, $p_t > 50 \,\text{GeV}$, $\not{\!\!E} > 100 \,\text{GeV}$, $|p_{\text{long}}/p_{\text{tot}}| < 0.9$ and an anti-b-tag. Because of the large mass difference between the two produced neutralinos $\tilde{\chi}_2^0$ and $\tilde{\chi}_4^0$, the signal typically has a relatively large total transverse momentum, so that the cut on p_t is increased to $50 \,\text{GeV}$ here. Moreover, one pair of jets, stemming from the $\tilde{\chi}_4^0$ decay, has to have an invariant mass equal to the Z-boson mass, while the other jet pair, associated with the $\tilde{\chi}_2^0$, must have an invariant mass smaller then the Z-boson mass. Therefore the cuts $|m_{j_1 j_2} - M_Z| < 10 \,\text{GeV}$ and $M_Z - m_{j_3 j_4} > 10 \,\text{GeV}$ are very effective.

These cuts reduce the background to $B = 61$ events, while $S = 430$ signal events are retained. Therefore the total production cross-section can be extracted with a statistical error of $\delta\sigma_{24}^0 = 5.4\%$.

As before, more information can be extracted from the decay distributions. The energy spectra of the jet pairs stemming from the $\tilde{\chi}_2^0$ and $\tilde{\chi}_4^0$ decay have distinct endpoints given
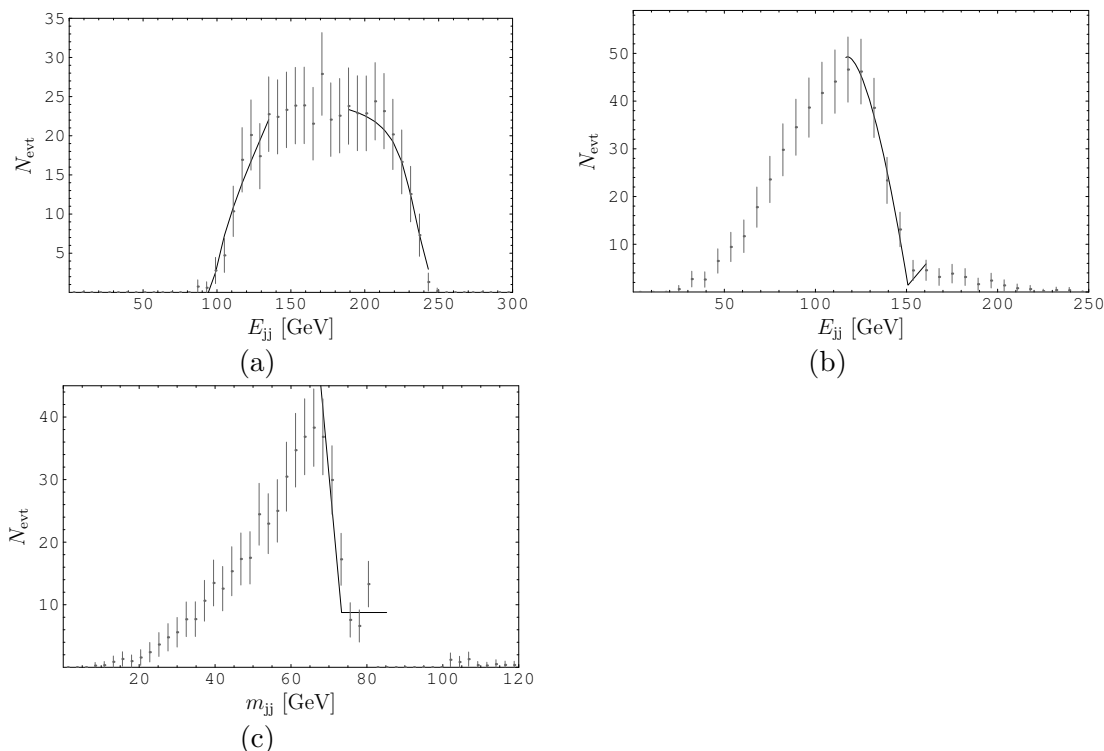
Figure 7: (a) Fit to the energy spectrum of the jet pair originating from $\tilde{\chi}_4^0$ decay, with $m_{jj} \sim M_{\mathrm{Z}}$. (b) Fit to the energy spectrum of the jet pair originating from $\tilde{\chi}_2^0$ decay, with $m_{jj} \ll M_{\mathrm{Z}}$. (c) With to invariant mass spectrum of the jet pair from $\tilde{\chi}_2^0$ decay.

by

$$
E_{\mathrm{max},2} = \frac{m_{\tilde{\chi}_2^0}^2 - m_{\tilde{\chi}_4^0}^2 - 2m_{\tilde{\chi}_1^0}^2\sqrt{s} + s}{2\sqrt{s}},
$$

$$
\begin{aligned}
E_{\mathrm{min,max},4} = \frac{1}{4m_{\tilde{\chi}_4^0}^2\sqrt{s}} \Big(& m_{\tilde{\chi}_4^0}^4 - m_{\tilde{\chi}_2^0}^2 m_{\tilde{\chi}_4^0}^2 + m_{\tilde{\chi}_4^0}^2 M_{\mathrm{Z}}^2 - m_{\tilde{\chi}_2^0}^2 M_{\mathrm{Z}}^2 + m_{\tilde{\chi}_4^0}^2 s + M_{\mathrm{Z}}^2 s \\
& - m_{\tilde{\chi}_1^0}^2 (m_{\tilde{\chi}_4^0}^2 - m_{\tilde{\chi}_2^0}^2 + s) \mp \sqrt{\lambda(m_{\tilde{\chi}_4^0}^2, m_{\tilde{\chi}_1^0}^2, M_{\mathrm{Z}}^2)\,\lambda(m_{\tilde{\chi}_2^0}^2, m_{\tilde{\chi}_4^0}^2, s)} \Big).
\end{aligned}
\tag{3.24}
$$

In addition, the invariant mass of the jet pair from $\tilde{\chi}_2^0$ has a maximum value corresponding to the mass difference of the neutralinos $\tilde{\chi}_2^0$ and $\tilde{\chi}_1^0$,

$$
m_{\mathrm{jj,max},2} = m_{\tilde{\chi}_2^0} - m_{\tilde{\chi}_1^0},
\tag{3.25}
$$

All these kinematic edges can be fitted with simple functions, as shown in figure 7, with the result

$$
m_{\tilde{\chi}_2^0} = 106.6^{+12}_{-17}\ \mathrm{GeV}, \qquad m_{\tilde{\chi}_4^0} = 278.0^{+25}_{-18}\ \mathrm{GeV}, \qquad m_{\tilde{\chi}_1^0} = 33.3^{+12}_{-17}\ \mathrm{GeV}.
\tag{3.26}
$$

As for the case of $\tilde{\chi}_3^0 \tilde{\chi}_4^0$ production, the errors on the neutralino masses are relatively large.

3.3.7 Chargino $\tilde{\chi}_2^{\pm}$

Heavy charginos $\tilde{\chi}_2^{\pm}$ can be produced in association with light charginos $\tilde{\chi}_1^{\pm}$, $e^+e^- \to \tilde{\chi}_1^{\pm}\tilde{\chi}_2^{\mp}$. While the $\tilde{\chi}_1^{\pm}$ mainly decays into W bosons and the lightest neutralino $\tilde{\chi}_1^0$, the $\tilde{\chi}_2^{\pm}$ has a large branching ratio of 62% into $ZW^{\pm}\tilde{\chi}_1^0$ via the decay chains $\tilde{\chi}_2^{\pm} \to Z\tilde{\chi}_1^{\pm} \to ZW^{\pm}\tilde{\chi}_1^0$ and $\tilde{\chi}_2^{\pm} \to W^{\pm}\tilde{\chi}_3^0 \to ZW^{\pm}\tilde{\chi}_1^0$. These decay channels for the charginos lead to three gauge bosons and missing energy from the neutralinos. The gauge bosons themselves can decay through various channels, but a good compromise between large statistics and clean leptonic final states is obtained by requiring one W boson to decay leptonically, and the other W and the Z going into a hadronic final state. The final state signature is then characterized by four jets, one lepton and missing energy, $e^+e^- \to \tilde{\chi}_1^{\pm}\tilde{\chi}_2^{\mp} \to ZW^+W^-\tilde{\chi}_1^0\tilde{\chi}_1^0 \to 4j\,l^{\pm}+\not{E}$. The signal can be enhanced by polarizing the beams with $P(e^+)/P(e^-) = $ right/left, see table 8.

The most relevant SM backgrounds are triple gauge boson processes, $e^+e^- \to W^+W^-Z$ and $t\bar{t}$ events. Production of heavy neutralino pairs can also lead to three gauge bosons in the final state, and thus is another important background.

After the standard cuts $p_t > 12\,\mathrm{GeV}$ and $\not{E} > 100\,\mathrm{GeV}$ and a bottom veto, a number of additional selection cuts has to be applied to reduce the backgrounds. Since the SM background, without neutralinos in the final state, tends to give more energy to the gauge bosons, it can be reduced by requiring the total hadronic energy to be $E_{\mathrm{had}} < 300\,\mathrm{GeV}$. The invisible neutralinos in the signal also lead to a large value for the invariant mass of the leptonic momentum and reconstructed missing 4-momentum, $m_{l\not{E}}$, so that the cut $m_{l\not{E}} > 150\,\mathrm{GeV}$ reduces the SM further. For the SM background, this invariant mass can also be reconstructed from the missing 3-momentum $\vec{\not{p}}$ only, by assuming that the missing energy originates from a neutrino, and it should be close the W mass. Therefore the cut $|m_{l\not{p}} - M_{\mathrm{W}}| > 10\,\mathrm{GeV}$ is also effective on the background. Furthermore, the signal is characterized by a large acoplanarity between the lepton and combined jet system, so that the cut $\cos\phi_{\mathrm{aco,lj}} > -0.7$ is useful. Finally, two of the jets have to combine to the invariant mass of the Z boson, while the other two jets have to combine to W mass, $|m_{j_1 j_2} - M_{\mathrm{Z}}| < 10\,\mathrm{GeV}$ and $|m_{j_3 j_4} - M_{\mathrm{W}}| < 10\,\mathrm{GeV}$. This removes most of $\tilde{\chi}_2^0\tilde{\chi}_4^0$ background and is also effective on $t\bar{t}$.

After application of these cuts, the SM background is removed to a negligible level, while still a sizeable contamination of background from $\tilde{\chi}_3^0\tilde{\chi}_4^0$ is left. In total $B = 245$ background events remain, compared to $S = 186$ events for the signal. Since the cross-section for the neutralino process can be measured independently, as described above, it can be subtracted, but the additional error from this procedure needs to be taken into account. The resulting expected precision for the $\tilde{\chi}_1^{\pm}\tilde{\chi}_2^{\mp}$ cross-section is $\delta\sigma_{12}^{\pm} = 13\%$.

For the chargino signal, the spectrum of the 4-jet invariant mass has an upper limit of $m_{\mathrm{inv,j,max}} = m_{\tilde{\chi}_2^{\pm}} - m_{\tilde{\chi}_1^0}$, which can be used to extract information about the heavy chargino mass. The neutralino background typically leads to slightly smaller 4-jet invariant masses, so that this upper edge is not contaminated. From a fit to the data, one obtains

$$m_{\mathrm{inv,j,max}} = 287.2^{+5.4}_{-4.2}\ \mathrm{GeV}, \tag{3.27}$$

which together with the $m_{\tilde{\chi}_1^0}$ mass measurement from the analysis of $\tilde{\chi}_1^+ \tilde{\chi}_1^-$ production directly translates into

$$m_{\tilde{\chi}_2^\pm} = 319.5^{+5.5}_{-4.3} \text{ GeV}. \tag{3.28}$$

3.3.8 Combination of sparticle measurements at ILC

Feeding in the precise measurement of the neutralino mass from the analysis of $\tilde{\chi}_1^+ \tilde{\chi}_1^-$ production, the masses of the heavier neutralinos from $\tilde{\chi}_2^0 \tilde{\chi}_4^0$ and $\tilde{\chi}_3^0 \tilde{\chi}_4^0$ production can be determined much more accurately,

$$m_{\tilde{\chi}_2^0} = 106.6^{+1.1}_{-1.3} \text{ GeV}, \qquad m_{\tilde{\chi}_3^0} = 181.5 \pm 4.9 \text{ GeV}, \qquad m_{\tilde{\chi}_4^0} = 278.0^{+2.5}_{-3.5} \text{ GeV}. \tag{3.29}$$

For the lightest neutralino and the charginos, the expected errors given in the previous sections are not improved by combining with the other neutralino observables, so that one obtains

$$m_{\tilde{\chi}_1^0} = 33.3^{+0.4}_{-0.3} \text{ GeV}, \qquad m_{\tilde{\chi}_1^\pm} = 164.98 \pm 0.05 \text{ GeV}, \qquad m_{\tilde{\chi}_4^0} = 319.5^{+5.5}_{-4.3} \text{ GeV}. \tag{3.30}$$

From a χ^2 fit to all mass and cross-section observables, constraints on the underlying neutralino and chargino parameters can be extracted. For completeness, we also allow a cubic singlet coupling κ as in the NMSSM. In the nMSSM, κ must be zero, but it is interesting not to impose this requirement a priori, but see how well it can be checked from an experimental analysis. The parameter κ enters in the (5,5)-entry of the neutralino mass matrix,

$$M_{\tilde{\chi}^0} = \begin{pmatrix} M_1 & 0 & -c_\beta s_W M_Z & s_\beta s_W M_Z & 0 \\ 0 & M_2 & c_\beta c_W M_Z & -s_\beta c_W M_Z & 0 \\ -c_\beta s_W M_Z & c_\beta c_W M_Z & 0 & \lambda v_s & \lambda v_2 \\ s_\beta s_W M_Z & -s_\beta c_W M_Z & \lambda v_s & 0 & \lambda v_1 \\ 0 & 0 & \lambda v_2 & \lambda v_1 & \kappa \end{pmatrix}, \tag{3.31}$$

The possible measurements at the ILC analyzed here comprise mass measurements for four neutralino and two chargino states, as well as four cross-section measurements. They can be used to derive bounds on the seven unknown parameters in the neutralino and chargino mass matrices. Furthermore, the cross-section measurements also allow to place limits on the masses of the sneutrino and selectron, which appear in the t-channel of the chargino and neutralino production diagrams. Based on the analysis of the expected experimental error in the previous subsections, the following constraints on the underlying parameters are obtained:

$$\begin{aligned} M_1 &= (122.5 \pm 1.3) \text{ GeV}, & |\kappa| &< 2.0 \text{ GeV}, & m_{\tilde{\nu}_e} &> 5 \text{ TeV}, \\ M_2 &= (245.0 \pm 0.7) \text{ GeV}, & \tan\beta &= 1.7 \pm 0.09, & m_{\tilde{e}_R} &> 1 \text{ TeV}. \\ |\lambda| &= 0.619 \pm 0.007, & |\phi_M| &< 0.32, \\ v_s &= (-384 \pm 4.8) \text{ GeV}, \end{aligned} \tag{3.32}$$

The extraction of the parameters λ and v_s is strongly correlated, which can be understood by the fact that these parameters enter in the chargino and neutralino mass matrices mainly

through the combination $\mu = -\lambda v_{\mathrm{s}}$. As a consequence, the effective parameter μ itself is determined more precisely than v_{s}, $\mu = (238 \pm 1.2)$ GeV.

The results of the fit show that the sizable value of the trilinear Higgs coupling λ can be established, which is a necessary requirement to avoid the Higgs mass bounds and allow a successful baryogenesis in singlet extensions of the MSSM. Furthermore, a strong upper bound on the value of κ is obtained, which allows a distinction between the two typical types of singlet extensions, the NMSSM and the nMSSM.

4. Cosmological implications

The cosmological energy density of the main components of matter, baryons and dark matter, is measured with a remarkable precision [39]. In units of the critical density[5]

$$\Omega_{\mathrm{B}} h^2 = 0.02233^{+0.00124}_{-0.00172},$$
$$\Omega_{\mathrm{CDM}} h^2 = 0.1106^{+0.0113}_{-0.0151},$$

at 95% CL. According to the observations, the baryon density is dominated by baryons while anti-baryons are only secondary products from high energy processes. The source of this baryon-anti-baryon asymmetry and the nature of dark matter are major puzzles of particle and astrophysics.

Assuming that inflation washes out any initial baryon asymmetry after the Big Bang, a dynamic mechanism should generate the asymmetry after inflation. Most microscopic mechanisms for baryogenesis fulfill the three Sakharov requirements:

- baryon number (B) violation,

- CP violation, and

- departure from equilibrium.

These conditions are satisfied in the supersymmetric extensions of the Standard Model during the electroweak phase transition. This is the basis for electroweak baryogenesis (EWBG). Baryon number violation occurs in the nMSSM due to quantum transitions between inequivalent SU(2) vacua that violate the sum of baryon and lepton number $B + L$. When the electroweak phase transition is first order, bubbles of broken phase nucleate within the symmetric phase as the Universe cools below the critical temperature. These provide the necessary departure from equilibrium. To generate the observed baryon asymmetry the electroweak phase transition has to be strongly first order. For light Higgs bosons, a first order phase transition can be induced by the trilinear coupling between the singlet and Higgs fields [16]. Such a term produces a sufficient contribution to the cubic term in the one-loop effective potential that is responsible for making the phase transition first order.

---

[5]$\rho_c = 3H_0^2/(8\pi G_N)$ where $H_0 = h \times 100\ km/s/Mpc$ is the present value of the Hubble constant, $h = 0.709^{+0.024}_{-0.032}$, and G_N is Newton's constant.

As discussed in section 2 the lightest superpartner in the nMSSM is typically the lightest neutralino, with a mass below about 60 GeV (for λ below the perturbative bound) and a sizeable singlino component. Cosmologically this signals danger since a light, stable particle with very weak gauge couplings may have a relic abundance substantially above the observed amount. But if the lightest neutralino is able to annihilate sufficiently well, this particle is a good dark matter candidate [63].

For values of $\tan\beta$ and λ consistent with the perturbative limit, the lightest neutralino also acquires some higgsino component. Since its light mass allows for efficient annihilation nearby the Z^0 resonance, its relic density spans a wide range as the function of its mass. While the s-channel Z^0 exchange is the dominant annihilation mode, there are also contributions from s-channel Higgs boson exchanges generated by the trilinear singlet-Higgs-Higgs term of the superpotential. These contributions tend to be significant only near the corresponding mass poles [16].

When the neutralino relic density is consistent with the astrophysical constraints, and the model parameters with electroweak baryogenesis and the perturbative bound, the next lightest supersymmetric particle (NLSP) is always at least 15 percent (and frequently more than 25 percent) heavier than the LSP, assuring that the co-annihilation contribution is strongly Boltzmann-suppressed. Moreover, since the NLSP is typically a neutralino with large bino component, which has small couplings to the gauge bosons, the co-annihilation cross section between the LSP and NLSP is suppressed even further and does not play any role in the following discussion.

4.1 Dark matter relic density

The relic abundance of neutralinos is computed numerically by solving the Boltzmann equation for the number density of the supersymmetric particles. The complex phase of λ enters our relic density calculation directly via the couplings and indirectly through the masses of the neutralinos and charginos. After diagonalizing the gaugino, sfermion and Higgs mass matrices, we calculate the annihilation cross sections with complex couplings. In doing this, we follow techniques used in refs. [64, 65]. The co-annihilation processes are checked to contribute insignificantly to the final result.

After superpartners are discovered and their properties being measured at colliders one has to assure the consistency of the collider and astrophysical data. A crucial part of this is to ensure that the lightest, stable supersymmetric particle provides a reasonable amount of the observed cold dark matter.

As discussed before, the LHC will restrict some of the soft supersymmetric parameters within certain ranges. Using these ranges, we can calculate the possible amount of neutralino dark matter, Ωh^2, within the given supersymmetric model. In this section we use our results obtained above for scenario A. To obtain an estimate of the precision the LHC can determine Ωh^2 in the nMSSM, we randomly sampled the nMSSM parameter space in the following parameter region:

$$0 < M_1 < 200 \text{ GeV}, \ 100 \text{ GeV} < M_2 < 300 \text{ GeV}, \ 0 < |\lambda| < 1, \ -\pi < \phi_{\mathrm{M}} < \pi,$$
$$-1000 \text{ GeV} < v_{\mathrm{s}} < -100 \text{ GeV}, \ -1000 \text{ GeV} < \kappa < 1000 \text{ GeV}, \ 0 < \tan\beta < 30. \quad (4.1)$$
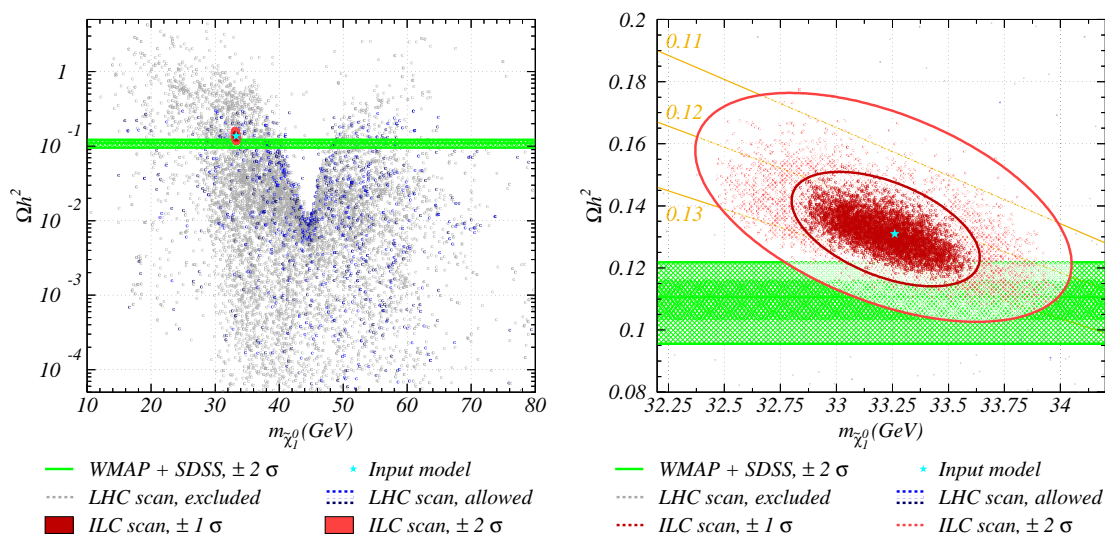
Figure 8: Neutralino relic density as the function of the neutralino mass. Dark (light) blue dots represent the 1 (2) σ precision of the LHC determination of Ωh^2, while gray dots would be allowed by LHC data, but are excluded by current low-energy and astrophysical bounds. Red dots show the expected ILC precision for the examined model point. The present WMAP and SDSS combined 2 σ limits are shown by the green shaded band. The right frame shows the ILC scan in more details, with contours of constant values of the mixing parameter $\left(|N_{14}|^2 - |N_{13}|^2\right)$ indicated by the yellow lines.

Additionally, for the first generation sleptons, we use the following ranges both in our LHC and ILC scans:

$$0.5 \text{ TeV} < M_{e_R} < 10 \text{ TeV}, \quad 0.5 \text{ TeV} < M_{L_1} < 10 \text{ TeV}. \tag{4.2}$$

The results of this scan, within the parameter region that would be allowed by LHC measurements at the 1 σ level, are projected on the lightest neutralino relic density vs. mass plane in figure 8.

Blue (gray) dots represent models that are (not) allowed by either the WMAP, the electron EDM, or WIMP direct detection limits. The dark (light) blue dots show the 1 (2) σ precision of the LHC determination of Ωh^2. All blue points satisfy all known low energy, collider and astrophysical constraints. Among these, the most stringent bounds come from the LEP and Tevatron Higgs and sparticle mass limits, WMAP, and the direct WIMP detection experiments.

Figure 8 (left) clearly demonstrates that from LHC measurements no meaningful constraints on Ωh^2 can be derived. In contrast, as depicted in figure 8 (right), the ILC 1 σ precision, indicated by the dark red dots, is comparable to the present WMAP and SDSS combined 2 σ limits, shown by the green shaded band. Even at the 2 σ level, the ILC could provide important information. In more quantitative terms the constraints on the neutralino relic density from the ILC measurements are

$$0.105 < \Omega h^2 < 0.178. \qquad (2\sigma) \tag{4.3}$$

As can be seen from figure 8, the computed dark matter density is strongly correlated with the lightest neutralino mass. Therefore a precise measurement of $m_{\tilde{\chi}_1^0}$ is essential for the accurate prediction of Ω_{CDM}. As shown in the previous section, for the sample scenario A the neutralino mass can be constrained best from chargino observables, in particular using a chargino threshold scan.

Once the neutralino mass from the ILC and their relic abundance from astrophysical measurements are known with the precision indicated by figure 8, we can even extract information on the neutralino mixing matrix. This is possible because the relic density of neutralinos depends only on the neutralino mass and the $Z\tilde{\chi}_1^0\tilde{\chi}_1^0$ coupling, given by eq. (3.14). Constant contours of $\left(|N_{14}|^2 - |N_{13}|^2\right)$ in figure 8 indicate the precision at which this coupling can be extracted from the combination of collider and astrophysical data in the ILC era. While in principle it is possible to determine the neutralino mixing matrix completely from ILC data alone by reconstructing the neutralino mass matrix, the combination of collider and astrophysical data allows to extract information about the mixings without having to assume the particle content of the nMSSM/NMSSM. This can provide an interesting cross-check about the structure of the underlying model.

The accuracy in the interplay of the collider and astrophysical measurements can be considered spectacular. If a consistency of the measurements as shown in figure 8 (right) were demonstrated it would be an impressive test of this model. On the other hand, it is worth noting that an inconsistency of the ILC and astrophysical data would pose an interesting, and potentially fruitful, situation. A collider indication of higher than WMAP or PLANCK allowed dark matter density, for example, may signal non-standard cosmology. Such an inconsistency could be the first sign that the temperature of the radiation dominated epoch before Big-Bang nucleosynthesis is not high enough for neutralinos to reach kinetic and chemical equilibrium. Alternatively, the entropy of matter and radiation may not be conserved or late production of entropy tips its balance. If instead the relic density implied by collider data were too small then this could be interpreted as a hint of additional dark matter constituents besides the neutralino. In either case, the ILC has a potential to uncover far reaching cosmic connections.

4.2 Dark matter direct detection

Another important requirement is the consistency of collider and dark matter direct detection data. Direct detection experiments search for weakly interacting massive particles via their elastic scattering off nuclei by measuring the nuclear recoil. There are numerous existing and future experiments engaged in this search [66]. These experiments uniformly express their observations in terms of the neutralino-proton scattering cross section. Most of the current direct detection experiments are primarily sensitive to scalar interactions of neutralinos with nuclei, and typically the most stringent limits are the spin independent ones. This is because for heavy nuclei the spin independent cross section, being proportional to the squared mass of the target nucleus, is highly enhanced compared to the spin dependent one.

While both spin dependent and independent scattering rates receive contributions from s-channel squark exchanges, the dominant processes are t-channel Z boson and Higgs
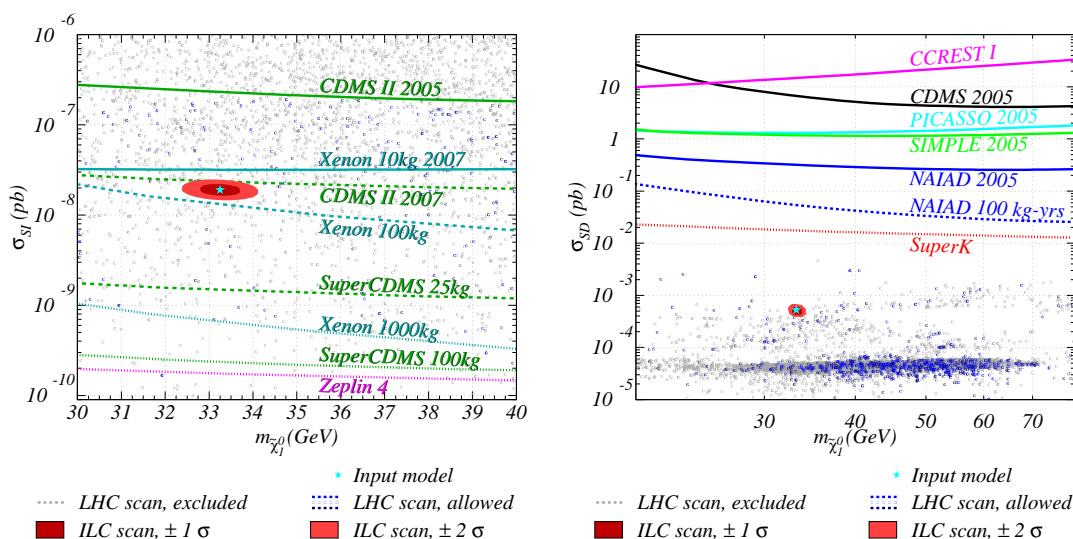
Figure 9: Left frame: Spin independent neutralino-proton elastic scattering cross sections as a function of the (lightest) neutralino mass. Blue and gray dots show the results of the LHC scan projected to this plane. Red dots correspond to the ILC scan. The regions above the various curves are excluded by the indicated experiments. Right frame: Spin dependent neutralino-proton elastic scattering cross section compared to various direct detection experiments, and to SuperK indirect limits for neutrinos stemming from neutralino annihilation in the Sun. The red region indicates the prediction from ILC measurements.

exchange for spin dependent and independent interactions, respectively. Due to close to resonant Z-exchange the spin dependent scattering cross section is enhanced in the nMSSM. However, as a result of the small $Z\tilde{\chi}_1^0\tilde{\chi}_1^0$ coupling, the cross section will not be within reach of the next generation of direct detection experiments.

Figure 9 shows the neutralino-proton elastic scattering cross sections in the nMSSM as the function of the (lightest) neutralino mass. The results of our LHC (blue and gray dots) and ILC (red dots) scans are projected to this plane, and the regions above the various curves are excluded by each indicated experiment. Due to the large singlino component in $\tilde{\chi}_1^0$, the spin dependent neutralino-proton elastic scattering cross section is very small. The spin independent cross section, on the other hand, is enhanced through the sizeable scalar self-coupling λ, which generates the dominant contribution for the coupling of $\tilde{\chi}_1^0$ to the CP-even Higgs bosons. As the left frame of figure 9 shows, the current and next generation direct detection experiments can already test what role the nMSSM plays in the explanation of dark matter, see also ref. [67]. In particular, SuperCDMS and Xenon should be able to discover or rule out benchmark point A in the near future.

The right frame of figure 9 shows the results of the scan for the spin dependent neutralino-proton elastic scattering cross section σ_{SD}. The sensitivity of many spin dependent direct detection experiments [68], together with the SuperK limit is also shown. Contrary to the spin independent case, the present and near future direct detection experiments fall short of observing this scenario. The strongest limit on σ_{SD} presently comes from the SuperK search for an excess of high energy muon neutrinos from WIMP annihi-

lation in the Sun. Since, among other astrophysical quantities, this neutrino flux depends on σ_{SD}, the SuperK measurement is able to constrain it from above [69]. In the future, the most stringent bounds on σ_{SD} may also come from indirect detection experiments. Unfortunately, the sensitivity of the IceCUBE neutrino telescope has only sensitivity for energies above the maximum energy of neutrinos expected from the nMSSM scenario, so we do not expect a strong constraint from it.

One should keep in mind that in general the direct detection cross sections depend on the CP-violating gaugino phase ϕ_M, but at present there are large theoretical uncertainties associated with the determination of the value of ϕ_M preferred for baryogenesis. The choice $\phi_M = 0.14$ in the benchmark scenario A serves as a guideline, but the correct value might differ by a factor of two. When changing the phase to the rather extreme case $\phi_M \approx \pi$, the spin independent cross section increases moderately by roughly 50%. Thus our main conclusions, that σ_{SI} can be tested in the near future, while σ_{SD} is likely out of reach of all planned experiments, remain the same irrespective of the value of ϕ_M.

The relatively small dependence of the direct detection cross section on the phase ϕ_M of the gaugino mass parameters can be undertstood by observing that the lightest neutralino is mainly singlino and has only a small gaugino component. As pointed out in section 2.2, however, a relevant phase can also appear in the singlet-Higgs sector, for example in the parameter a_λ. Such a complex phase could have a much stronger impact on the direct detection scattering cross sections, depending on the value of $\arg(a_\lambda)$. It would be interesting to study this possibility and its interrelation with the generation of baryon asymmetry. We reserve such a study for a future investigation.

4.3 Baryogenesis

As shown in the previous section, the measurements of the chargino and neutralino sector at the LHC and the ILC provide a test of the presence of light charginos and neutralinos, necessary to generate the dark matter relic density. In order to probe the mechanism of electroweak baryogenesis with collider results, two conditions need to be tested: the type of the electroweak phase transition must be strongly first order, and there must be CP violating processes active during this phase transition.

In our benchmark scenario, CP violation is introduced in the baryon-number generating processes through light chargino currents. For this mechanism, the charginos need to be light enough so that they are not decoupled at the temperature of electroweak symmetry breaking. Using the experimental results from LHC and ILC, see eqs. (3.13) and (3.32), the existence of sufficiently light chargino can easily be tested. In addition, the presence of a complex CP-violating parameter in the chargino sector is required for baryogenesis. However, even with the high precision of ILC, only an upper bound on the phase ϕ_M of the gaugino mass parameters can be obtained, see eq. (3.32).

To test the other condition, the strength of the first order phase transition, the Higgs sector of the model needs to be analyzed. The strength of the phase transition can be calculated from the effective Higgs potential, see e.g. [16]. It depends crucially on the supersymmetry breaking term m_s^2 and a_λ, which are not constrained by the analysis of charginos and neutralinos. However, as we will show below, information about these pa-

rameters may be obtained by the precise determination of the CP-even Higgs boson masses, which would be possible at the ILC.

From the condition of the strongly first order phase transition, one finds the following conditions on the parameters of the Higgs potential [16]:

$$
\begin{aligned}
m_{\mathrm{s}}^2 &= -a_\lambda v_1 v_2/v_{\mathrm{s}} - t_{\mathrm{s}}/v_{\mathrm{s}} - \lambda^2 v^2 \\
&\in \{(50 \text{ GeV})^2, (200 \text{ GeV})^2\} \qquad \text{for perturbative } \lambda \lesssim 0.8,
\end{aligned} \tag{4.4}
$$

$$
|D| \equiv \left| \frac{1}{m_{\mathrm{s}}^2 \sqrt{\lambda^2/4 \, \sin^2 2\beta + \bar{g}^2/8 \, \cos^2 2\beta}} \left(\lambda^2 t_{\mathrm{s}}/m_{\mathrm{s}} - a_\lambda \sin\beta \cos\beta \, m_{\mathrm{s}} \right) \right| \gtrsim 1, \tag{4.5}
$$

where we have introduced the quantity D for abbreviation.

As stressed above, constraints on these parameters can be obtained from the Higgs masses. To relate the masses to the underlying parameters, the Higgs mixing matrices need to be reconstructed. Following the discussion in section 2.2, we have assumed CP-conservation in the Higgs sector, to that mixing occurs only between Higgs boson with the same CP quantum numbers. The heavy Higgs states $S_3, P_2, H^\pm$ with masses of the order of M_{A} are not within reach of either the LHC or ILC (the most promising discovery channels for heavy Higgs bosons at the LHC are suppressed due to the small value of $\tan\beta$ in our scenario). From the fact that the charged Higgs boson would not be observed at the ILC with $\sqrt{s} = 1$ TeV, one could derive the limit $M_{\mathrm{A}} > 500$ GeV. Due this bound the heavy CP-even Higgs boson is essentially decoupled, so that the lightest CP-even Higgs has only sizeable mixing with the second-lightest CP-even Higgs. Both of these masses can be measured at ILC. The mass matrix is

$$
M_{\mathrm{S}_{1,2}}^2 = \begin{pmatrix} M_{\mathrm{Z}}^2 \cos^2 2\beta + \lambda^2 v^2 \sin^2 2\beta & v(a_\lambda \sin 2\beta + 2\lambda^2 v_{\mathrm{s}}) \\ v(a_\lambda \sin 2\beta + 2\lambda^2 v_{\mathrm{s}}) & m_{\mathrm{s}}^2 + \lambda^2 v^2 \end{pmatrix} + \Delta M_{\mathrm{S}_{1,2}}^2, \tag{4.6}
$$

where $\Delta M_{\mathrm{S}_{1,2}}^2$ represents radiative corrections. The largest corrections stem from top-stop loops, but they are relatively small except for the (1,1)-entry,

$$
\Delta M_{\mathrm{S}_{1,2}}^2 \equiv \begin{pmatrix} \Delta_{S11} & \Delta_{S12} \\ \Delta_{S21} & \Delta_{S22} \end{pmatrix} \approx \begin{pmatrix} \Delta_{S11} & 0 \\ 0 & 0 \end{pmatrix}, \quad \text{with } \Delta_{S11} \approx \frac{3}{8\pi^2} \frac{m_{\mathrm{t}}^4}{v^2} \log \frac{m_{\tilde{t}_1}^2 m_{\tilde{t}_2}^2}{m_{\mathrm{t}}^4}. \tag{4.7}
$$

A rough constraint on m_{s} can be obtained by considering that one of the two eigenvalues of the mass matrix is always larger than the diagonal entries of the matrix, while the other eigenvalue is smaller than the diagonal entries. Ergo:

$$
M_{S1}^2 < m_{\mathrm{s}}^2 + \lambda^2 v^2 < M_{S2}^2. \tag{4.8}
$$

Using the uncertainties for λ from the fit to the ILC measurements in the neutralino sector, one gets

$$
(41 \pm 3)^2 \text{ GeV}^2 \lesssim m_{\mathrm{s}}^2 \lesssim (114 \pm 1)^2 \text{ GeV}^2, \tag{4.9}
$$

compared to the input value of $m_{\mathrm{s}} = 106.5$ GeV. Thus this very crude estimate is already sufficient to establish m_{s} in the required range.

A more detailed determination would be possible by looking at the whole matrix eq. (4.6), including full one-loop corrections [13], not only the leading term in eq. (4.7). The radiative corrections add an additional uncertainty due to the parametric dependence on the stop masses $m_{\tilde{t}_{1,2}}$, A_{t} and M_{A}.

These parameters would need to be constrained from experiment. While in our scenario the stops are too heavy to be produced at a 1 TeV linear collider, one can try to search for them at the LHC. The study of ref. [70] finds that a signal from decays of gluinos into stops can be identified with a dedicated analysis. Ref. [70] also proposes a strategy to measure the stop mass, although a translation to our scenario is not straightforward. Nevertheless, to exemplify the improvement that such a stop analysis could bring for the understanding of the Higgs sector, we here simply assume that the stop masses can be measured with an error of $\delta m_{\tilde{t}} = 50\,\mathrm{GeV}$. For the parameter A_{t} the situation is more difficult, since it cannot be measured directly. However, given that in our scenario there is only a relatively small difference between the two stop masses, which we assume can be measured, one can infer that $A_{\mathrm{t}} \lesssim 500$ GeV. As far as M_{A} is concerned, only a lower limit of $500\,\mathrm{GeV}$ could be obtained in our scenario, as pointed out above. With these constraints, and taking into account the expected errors for all relevant masses and parameters, the full one-loop analysis yields

$$a_\lambda = (373^{+17}_{-21})\ \mathrm{GeV}, \qquad\qquad m_{\mathrm{s}} = (106 \pm 18)\ \mathrm{GeV},$$
$$t_{\mathrm{s}}^{1/3} = (156^{+25}_{-39})\ \mathrm{GeV}, \qquad\qquad |D| \sim 1.0 \pm 0.65. \tag{4.10}$$

Note that the parameters a_λ and m_{s} can be constrained very precisely from the measurement of Higgs masses at the ILC. On the other hand, the necessary condition $|D| > 1$ cannot be proven with sufficient precision, although the result in eq. 4.10 is consistent with this condition.

In summary, measurements at future colliders can allow us to establish the chargino and Higgs mass parameters to be in the range required for electroweak baryogenesis in the nMSSM, but they do not seem sensitive enough to yield definitive answers to the questions of the first order phase transition and of the presence of additional CP violation.

4.3.1 Electron electric dipole moment

A necessary requirement of the electroweak baryogenesis scenario is the presence of non-vanishing CP-violating phases in the chargino-neutralino sector. In this work, we have assumed that these phases are associated with the gaugino sector of the theory. However, the collider, or the dark matter constraints described in the previous sections are not sufficient to determine the exact value of the CP-violating phases necessary for the generation of the baryon-antibaryon asymmetry. An important question is if one could obtain information about these phases from the measurement of, for instance, the electron electric dipole moment. It is advantageous to use the electron EDM since it is precisely measured, has relatively low theoretical uncertainties, and for the phases relevant to the model under study gives the strongest constraint. Since both the baryon asymmetry and the electron EDM increase with $\sin(\phi_{\mathrm{M}})$, the electron electric dipole moment d_e provides an important constraint on the realization of this electroweak baryogenesis scenario.
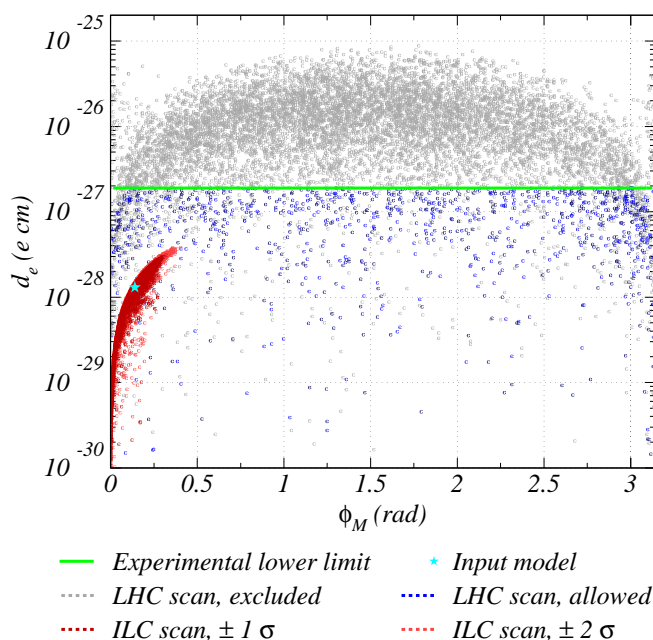
Figure 10: Comparison of the current bound on the electron electric dipole moment with parameter regions allowed by expected LHC and ILC measurements for the scenario A. The results are given as a function of the complex phase $\phi_{\rm M}$.

For non-vanishing phases in the gaugino sector, the supersymmetric contribution to d_e may become large and severe limits on the nMSSM parameter space can be obtained. Figure 10 demonstrates that most of the LHC scan, for which $\phi_{\rm M}$ deviates substantially from zero or π, is excluded by the present 2 sigma upper limit $|d_e| < 1.9 \times 10^{-27}$ e cm. Since neither the LHC nor the ILC will detect the first generation sleptons if their masses are large, we allowed these masses to vary in the scans in a wide range: $1 < M_{e_R} < 10$ TeV, $2.5 < M_{L_1} < 10$ TeV.[6] For the LHC only those models survive the $|d_e|$ limit which either have small values of $\phi_{\rm M}$, very large values of the slepton masses, or where the one and two loop contributions to d_e accidentally cancel. Unfortunately, since this cancellation can happen at any value of $\phi_{\rm M}$, the EDM limit combined with the LHC data cannot shed light on the actual value of the phase $\phi_{\rm M}$.

New experiments have been proposed which are expected to improve the electron EDM limits by orders of magnitude in the next few years [71, 72]. If baryogenesis is driven by a single gaugino phase of the nMSSM such as studied in this work, then a non-vanishing value of d_e will probably be measured by the time of the ILC operation as scenario A suggests.

---

[6]Barring accidental cancellations between different contributions, smaller values are only allowed by the present EDM limits if the phase $\phi_{\rm M}$ is very small. In principle this case could not be excluded by LHC data alone, since neither the slepton masses nor the CP-violating phase can be well constrained. However, as can be seen in figure 10, even after imposing these ad-hoc bounds on the slepton masses, the LHC data would allow nMSSM scenarios for which the value of the electron EDM varies over several orders of magnitude. Therefore the parameter space scan presented here should give a representative picture of the information that may be obtained after running the LHC.

This can even happen if the first generation sleptons are very heavy, as shown by the case of the input model A, where the first generation sleptons are fixed at $O(10\,TeV)$. If an electron EDM is measured, the indirect ILC determination of d_e will also be an essential cross check confirming the nMSSM. According to figure 10, the ILC data alone will be able to constrain $|\phi_{\mathrm{M}}|$ below about 0.3 and $|d_e|$ below about 5×10^{-28} e cm. The correlation between $|d_e|$ and $|\phi_{\mathrm{M}}|$ is strong in the relevant $\phi_{\mathrm{M}} \sim 0.1$ region. Utilizing this, even a 50% measurement of $|d_e|$ combined with the ILC data will be able to constrain ϕ_{M} in a ± 0.15 window.

4.3.2 Comment about parameter space for CP violation

In the previous sections we have made the simplifying assumption that the only CP-violating parameter beyond the CKM matrix is a common phase of the gaugino mass parameters $\phi_{\mathrm{M}} \equiv \phi_{\mathrm{M}_1} = \phi_{\mathrm{M}_2} = \phi_{\mathrm{M}_3}$. However, as pointed out in section 2, the general nMSSM with minimal flavor violation can have 13 complex CP-violating parameters in total, four of which can be relevant for electroweak baryogenesis. These four independent parameters can be chosen to be M_1, M_2, a_λ and A_{t}. For illustration, here we list the different scenarios that are possible if these phases are allowed to be non-zero. A more detailed investigation of these scenarios would be beyond the scope of this paper and has to be performed elsewhere.

Gaugino phases without gaugino unification: In this case, the baryogenesis could be driven by bino currents, which are sensitive to the phase of M_1, while the phase of M_2 could be zero. While, depending on the mass pattern, this still could allow the generation of a sufficiently large baryon asymmetry [36], it would reduce the contribution to the EDMs. As a result, lower values of the slepton masses of the order of a few TeV would be allowed. The collider sensitivity to ϕ_{M_1} would be similarly weak as for the common gaugino phase ϕ_{M} discussed above, since one would rely on the same observables in the neutralino sector. Contrary to the MSSM, a phase in M_1 will have no sizeable effect on the dark matter annihilation, since in the nMSSM the LSP is expected to be mainly singlino.

Only CP-violating phase in a_λ: As shown in ref. [27], a sizeable phase in the Higgs sector could succesfully explain electroweak baryogenesis. With the freedom of R- and PQ-transformations, this phase could be attributed alternatively to a_λ, t_{s} or m_{12}, without changing the physics. In this situation, the EDM constraints from one-loop diagrams will be much weaker than for a gaugino phase, since one-loop diagrams with a Higgs boson are suppressed by an additional small Yukawa coupling. As a result, in this scenario, light slepton masses of a few hundred GeV would be allowed, which could be in reach of the LHC or ILC. This feature could be used to experimentally discriminate this scenario from a scenario with non-zero gaugino phases. For instance, if the LHC or ILC would discover selectrons, the present electron EDM limit would rule out phases in the gaugino sector that are large enough to explain electroweak baryogenesis (except for the possiblity of large cancellations between two contributions to the EDM). A CP-violating phase in the Higgs sector could lead to observable effects in Higgs production processes and decays. For example, mixing between CP-even and CP-odd Higgs states would enable the possibility to produce a third light Higgs boson ϕ_i in the process $e^+ e^- \to \phi_i Z$. A more conclusive answer

to this question would require further study. As pointed out in section 4.2, a complex phase of a_λ can also strongly affect the dark matter scattering cross sections and thus could relax the constraints coming from dark matter direct detection experiments.

Only CP-violating phase in A_t: If the only non-zero phase (in addition to the CKM matrix) was in the parameter A_t, it is unlikely that a sufficiently large baryon asymmetry could be generated, as experience from the MSSM shows [34 – 37]. It is however possible that a non-zero phase of A_t can exist in conjunction with other complex nMSSM parameters.

CP-violating phases in several parameters: When considering to most general scenario with CP-violating phases in multiple parameters, the interpretation of the EDM limits becomes more involved. From our analysis, the prospects for disentangling the complex parameters through collider data do not seem promising.

5. Conclusions

In this article, we have presented the phenomenological properties of the nMSSM, assuming the parameters to be close to the ones that lead to a solution of the dark matter and baryogenesis problems. A light neutralino and chargino spectrum appears under these conditions, that can be probed at the LHC and the ILC. At the LHC, however the detection of these weakly interacting particles becomes difficult, unless they are produced from the cascade decay of strongly interacting particles. In order to study the LHC phenomenology we have therefore assumed that the gluino is within the reach of the LHC, as suggested by gaugino mass unification, and that the third generation squarks are light, which is helpful in avoiding the suppression of the chiral charges necessary for baryogenesis. We have shown that, under these conditions a relatively good determination of the LSP and other neutralino masses may be obtained. However, the accuracy of these measurements is not sufficient to allow the computation of the neutralino relic density with any meaningful precision. A definitive probe of this model can only be done at the ILC. At the ILC, for a representative point, we have shown that both chargino and four of the five neutralino masses may be determined. The sparticle mass pattern leads to a good discrimination of this model from the MSSM, and even a distinction between the nMSSM and the NMSSM, which has a different singlet sector, is possible. Moreover, the mass measurements, together with the production cross section information, lead to a good discrimination of this model from the MSSM, and allow to compute reliably the annihilation cross section of the LSP, and thus to check the agreement needed for a successful explanation of the dark matter relic density.

The requirement of a sufficiently strong first order electroweak phase transition also translates in this model into the presence of a light singlet scalar, which mixes after electroweak symmetry breaking with the MSSM Higgs doublets. Consequently, two light CP-even Higgs scalars appear in the spectrum which couple with reduced couplings to the weak gauge bosons, and which decay predominantly into the LSP. These CP-even Higgs bosons may be searched for at the LHC and the ILC in the invisible decay channel. At the LHC, however, it will be difficult to discern between one or more invisibly decaying

Higgs bosons. A definitive scrutiny of this question may only be performed at the ILC, at which a good determination of the Higgs boson masses may be established. A light CP-odd Higgs boson also appears in the spectrum, of difficult detectability due to its strongly reduced couplings to the SM fermions. Nevertheless, the pattern of the two CP-even Higgs boson masses allows to distinguish the nMSSM Higgs sector from the MSSM. In addition, the mass measurements provide information about the parameters of the model relevant for a strong first order electroweak phase transition. Note that for this kind of analysis, we have shown that the large radiative corrections in the Higgs sector need to be under control, requiring some information about the superpartners of the top quark needs from measurements at LHC or ILC.

Finally, we have also investigated the constraints coming from the current direct detection searches for dark matter, as well as the prospects of a successful observation of the dark matter candidate of this model at future experiments. We have shown that the predominantly singlet component of the LSP makes its direct detection easier than in the MSSM for the spin independent channel, but more difficult for the spin depedent channel. For the spin independent case, the current and next generation experiments should be able to definitely probe this scenario. Similarly, assuming that the dominant phases are in the chargino sector, we have also investigated the bounds coming from the electron electric dipole moment. We have shown that, due to the small values of $\tan\beta$ necessary to realize this model, the EDM constraints become weaker than in the MSSM, and, again, this model may only be probed by next generation experiments. If the dominant phases are in the Higgs sector instead, the EDM bounds are even weaker. Such complex phases may also affect the predicted dark matter direct detection cross sections significantly. In this case additional information about CP-violation might be obtainable from collider data in the Higgs sector.

In summary, the nMSSM provides an exciting framework for addressing the problems of baryogenesis and dark matter. The properties of this model and role it plays in solving these problems could be probed with high precision at the next generation of laboratory experiments, and would allow us to make connections between laboratory and astrophysical observations at a new level of insight.

Acknowledgments

References

[1] H.P. Nilles, *Supersymmetry, supergravity and particle physics*, *Phys. Rept.* **110** (1984) 1;
H.E. Haber and G.L. Kane, *The search for supersymmetry: probing physics beyond the standard model*, *Phys. Rept.* **117** (1985) 75.

[2] S.P. Martin, *A supersymmetry primer*, `hep-ph/9709356`.

[3] A.G. Cohen, D.B. Kaplan and A.E. Nelson, *Progress in electroweak baryogenesis*, *Ann. Rev. Nucl. Part. Sci.* **43** (1993) 27;
M. Quirós, *Field theory at finite temperature and phase transitions*, *Helv. Phys. Acta* **67** (1994) 451;
V.A. Rubakov and M.E. Shaposhnikov, *Electroweak Baryon number non-conservation in the early universe and in high energy collisions*, *Usp. fiz. Nauk* **166** (1996) 493 [*Phys. Usp.* **39** (1996) 461] [`hep-ph/9603208`];
M. Carena and C.E.M. Wagner, *Electroweak baryogenesis and Higgs physics*, `hep-ph/9704347`;
A. Riotto, M. Trodden, *Recent progress in baryogenesis*, *Ann. Rev. Nucl. Part. Sci.* **49** (1999) 35 [`hep-ph/9901362`];
M. Quirós and M. Seco, *Electroweak baryogenesis in the MSSM*, *Nucl. Phys.* **81** *(Proc. Suppl.)* (2000) 63 [`hep-ph/9903274`].

[4] M. Carena, M. Quirós and C.E.M. Wagner, *Opening the window for electroweak baryogenesis*, *Phys. Lett.* **B 380** (1996) 81 [`hep-ph/9603420`];
M. Laine, *Effective theories of MSSM at high temperature*, *Nucl. Phys.* **B 481** (1996) 43 [`hep-ph/9605283`];
M. Losada, *High temperature dimensional reduction of the MSSM and other multi-scalar models*, *Phys. Rev.* **D 56** (1997) 2893 [`hep-ph/9605266`];
G.R. Farrar and M. Losada, *SUSY and the electroweak phase transition*, *Phys. Lett.* **B 406** (1997) 60 [`hep-ph/9612346`];
B. de Carlos and J.R. Espinosa, *The baryogenesis window in the MSSM*, *Nucl. Phys.* **B 503** (1997) 24 [`hep-ph/9703212`];
D. Bodeker, P. John, M. Laine and M.G. Schmidt, *The 2-loop MSSM finite temperature effective potential with stop condensation*, *Nucl. Phys.* **B 497** (1997) 387 [`hep-ph/9612364`];
M. Carena, M. Quirós and C.E.M. Wagner, *Electroweak baryogenesis and Higgs and stop searches at LEP and the Tevatron*, *Nucl. Phys.* **B 524** (1998) 3 [`hep-ph/9710401`];
M. Laine and K. Rummukainen, *The MSSM electroweak phase transition on the lattice*, *Nucl. Phys.* **B 535** (1998) 423 [`hep-lat/9804019`];
M. Losada, *The two-loop finite-temperature effective potential of the MSSM and baryogenesis*, *Nucl. Phys.* **B 537** (1999) 3 [`hep-ph/9806519`]; *Mixing effects in the finite-temperature effective potential of the MSSM with a light stop*, *Nucl. Phys.* **B 569** (2000) 125 [`hep-ph/9905441`];
M. Laine and M. Losada, *Two-loop dimensional reduction and effective potential without temperature expansions*, *Nucl. Phys.* **B 582** (2000) 277 [`hep-ph/0003111`];
M. Laine and K. Rummukainen, *Two Higgs doublet dynamics at the electroweak phase transition: a non-perturbative study*, *Nucl. Phys.* **B 597** (2001) 23 [`hep-lat/0009025`].

[5] C. Balázs, M. Carena and C.E.M. Wagner, *Dark matter, light stops and electroweak baryogenesis*, *Phys. Rev.* **D 70** (2004) 015007 [`hep-ph/0403224`];
C. Bálazs, M. Carena, A. Menon, D.E. Morrissey and C.E.M. Wagner, *The supersymmetric origin of matter*, *Phys. Rev.* **D 71** (2005) 075002 [`hep-ph/0412264`].

[6] V. Cirigliano, S. Profumo and M.J. Ramsey-Musolf, *Baryogenesis, electric dipole moments and dark matter in the MSSM*, *JHEP* **07** (2006) 002 [hep-ph/0603246].

[7] M. Carena et al., *Analyzing the scalar top co-annihilation region at the ILC*, *Phys. Rev.* **D 72** (2005) 115008 [hep-ph/0508152].

[8] Y. Grossman, T. Kashti, Y. Nir and E. Roulet, *Leptogenesis from supersymmetry breaking*, *Phys. Rev. Lett.* **91** (2003) 251801 [hep-ph/0307081];
G. D'Ambrosio, G.F. Giudice and M. Raidal, *Soft leptogenesis*, *Phys. Lett.* **B 575** (2003) 75 [hep-ph/0308031];
Y. Grossman, T. Kashti, Y. Nir and E. Roulet, *New ways to soft leptogenesis*, *JHEP* **11** (2004) 080 [hep-ph/0407063].

[9] Y. Grossman, R. Kitano and H. Murayama, *Natural soft leptogenesis*, *JHEP* **06** (2005) 058 [hep-ph/0504160];
A.D. Medina and C.E.M. Wagner, *Soft leptogenesis in warped extra dimensions*, *JHEP* **12** (2006) 037 [hep-ph/0609052].

[10] C. Panagiotakopoulos and K. Tamvakis, *Stabilized NMSSM without domain walls*, *Phys. Lett.* **B 446** (1999) 224 [hep-ph/9809475].

[11] C. Panagiotakopoulos and K. Tamvakis, *New minimal extension of MSSM*, *Phys. Lett.* **B 469** (1999) 145 [hep-ph/9908351].

[12] P. Fayet, *Supergauge invariant extension of the higgs mechanism and a model for the electron and its neutrino*, *Nucl. Phys.* **B 90** (1975) 104; *Spontaneously broken supersymmetric theories of weak, electromagnetic and strong interactions*, *Phys. Lett.* **B 69** (1977) 489.

[13] C. Panagiotakopoulos and A. Pilaftsis, *Higgs scalars in the minimal non-minimal supersymmetric standard model*, *Phys. Rev.* **D 63** (2001) 055003 [hep-ph/0008268].

[14] A. Dedes, C. Hugonie, S. Moretti and K. Tamvakis, *Phenomenology of a new minimal supersymmetric extension of the standard model*, *Phys. Rev.* **D 63** (2001) 055009 [hep-ph/0009125].

[15] J. Kang, P. Langacker, T.-j. Li and T. Liu, *Electroweak baryogenesis in a supersymmetric U(1)′ model*, *Phys. Rev. Lett.* **94** (2005) 061801 [hep-ph/0402086].

[16] A. Menon, D.E. Morrissey and C.E.M. Wagner, *Electroweak baryogenesis and dark matter in the NMSSM*, *Phys. Rev.* **D 70** (2004) 035005 [hep-ph/0404184].

[17] LEP WORKING GROUP FOR HIGGS BOSON SEARCHES collaboration, R. Barate et al., *Search for the standard model Higgs boson at LEP*, *Phys. Lett.* **B 565** (2003) 61 [hep-ex/0306033];
LEP2 Higgs Working Group, ALEPH, DELPHI, *L3 and OPAL experiments*, note LHWG-Note-2004-01, http://lephiggs.web.cern.ch/LEPHIGGS/papers/.

[18] R. Harnik, G.D. Kribs, D.T. Larson and H. Murayama, *The minimal supersymmetric fat Higgs model*, *Phys. Rev.* **D 70** (2004) 015002 [hep-ph/0311349];
A. Delgado and T.M.P. Tait, *A fat Higgs with a fat top*, *JHEP* **07** (2005) 023 [hep-ph/0504224];
P. Batra, A. Delgado, D.E. Kaplan and T.M.P. Tait, *Running into new territory in SUSY parameter space*, *JHEP* **06** (2004) 032 [hep-ph/0404251].

[19] M. Carena, A. Megevand, M. Quirós and C.E.M. Wagner, *Electroweak baryogenesis and new TeV fermions*, *Nucl. Phys.* **B 716** (2005) 319 [hep-ph/0410352];
J. Shu, T.M.P. Tait and C.E.M. Wagner, *Baryogenesis from an earlier phase transition*, *Phys. Rev.* **D 75** (2007) 063510 [hep-ph/0610375].

[20] G.F. Giudice and M.E. Shaposhnikov, *Strong sphalerons and electroweak baryogenesis*, *Phys. Lett.* **B 326** (1994) 118 [hep-ph/9311367].

[21] S.A. Abel, S. Sarkar and P.L. White, *On the cosmological domain wall problem for the minimally extended supersymmetric standard model*, *Nucl. Phys.* **B 454** (1995) 663 [hep-ph/9506359].

[22] J.R. Ellis, J.F. Gunion, H.E. Haber, L. Roszkowski and F. Zwirner, *Higgs bosons in a nonminimal supersymmetric model*, *Phys. Rev.* **D 39** (1989) 844.

[23] U. Ellwanger, *Radiative corrections to the neutral Higgs spectrum in supersymmetry with a gauge singlet*, *Phys. Lett.* **B 303** (1993) 271 [hep-ph/9302224];
T. Elliott, S.F. King and P.L. White, *Supersymmetric Higgs bosons at the limit*, *Phys. Lett.* **B 305** (1993) 71 [hep-ph/9302202]; *Squark contributions to Higgs boson masses in the next-to-minimal supersymmetric standard model*, *Phys. Lett.* **B 314** (1993) 56 [hep-ph/9305282]; *Radiative corrections to Higgs boson masses in the next-to-minimal supersymmetric standard model*, *Phys. Rev.* **D 49** (1994) 2435 [hep-ph/9308309];
P.N. Pandita, *One loop radiative corrections to the lightest Higgs scalar mass in nonminimal supersymmetric standard model*, *Phys. Lett.* **B 318** (1993) 338; *Radiative corrections to the scalar Higgs masses in a nonminimal supersymmetric standard model*, *Z. Physik* **C 59** (1993) 575;
S.W. Ham, S.K. Oh and B.R. Kim, *Absolute upper bound on the 1-loop corrected mass of S_1 in the NMSSM*, *J. Phys.* **G 22** (1996) 1575 [hep-ph/9604243].

[24] OPAL collaboration, G. Abbiendi et al., *Search for chargino and neutralino production at $\sqrt{s} = 192\,GeV$ to $209\,GeV$ at LEP*, *Eur. Phys. J.* **C 35** (2004) 1 [hep-ex/0401026].

[25] ALEPH collaboration, *Precision electroweak measurements on the z resonance*, *Phys. Rept.* **427** (2006) 257 [hep-ex/0509008].

[26] M. Pietroni, *The electroweak phase transition in a nonminimal supersymmetric model*, *Nucl. Phys.* **B 402** (1993) 27 [hep-ph/9207227];
A.T. Davies, C.D. Froggatt and R.G. Moorhouse, *Electroweak baryogenesis in the next to minimal supersymmetric model*, *Phys. Lett.* **B 372** (1996) 88 [hep-ph/9603388];
S.J. Huber and M.G. Schmidt, *Electroweak baryogenesis: concrete in a SUSY model with a gauge singlet*, *Nucl. Phys.* **B 606** (2001) 183 [hep-ph/0003122];
M. Bastero-Gil, C. Hugonie, S.F. King, D.P. Roy and S. Vempati, *Does LEP prefer the NMSSM?*, *Phys. Lett.* **B 489** (2000) 359 [hep-ph/0006198].

[27] S.J. Huber, T. Konstandin, T. Prokopec and M.G. Schmidt, *Electroweak phase transition and baryogenesis in the NMSSM*, *Nucl. Phys.* **B 757** (2006) 172 [hep-ph/0606298].

[28] B.C. Regan, E.D. Commins, C.J. Schmidt and D. DeMille, *New limit on the electron electric dipole moment*, *Phys. Rev. Lett.* **88** (2002) 071805.

[29] C.A. Baker et al., *An improved experimental limit on the electric dipole moment of the neutron*, *Phys. Rev. Lett.* **97** (2006) 131801 [hep-ex/0602020].

[30] A. Pilaftsis, *Higgs-mediated electric dipole moments in the MSSM: an application to baryogenesis and Higgs searches*, *Nucl. Phys.* **B 644** (2002) 263 [hep-ph/0207277].

[31] T. Ibrahim and P. Nath, *The neutron and the lepton edms in MSSM, large CP-violating phases and the cancellation mechanism*, *Phys. Rev.* **D 58** (1998) 111301 [hep-ph/9807501].

[32] S. Abel, S. Khalil and O. Lebedev, *EDM constraints in supersymmetric theories*, *Nucl. Phys.* **B 606** (2001) 151 [hep-ph/0103320].

[33] D. Chang, W.-F. Chang and W.-Y. Keung, *New constraint from electric dipole moments on chargino baryogenesis in MSSM*, *Phys. Rev.* **D 66** (2002) 116008 [`hep-ph/0205084`].

[34] M. Carena, M. Quirós, A. Riotto, I. Vilja and C.E.M. Wagner, *Electroweak baryogenesis and low energy supersymmetry*, *Nucl. Phys.* **B 503** (1997) 387 [`hep-ph/9702409`];
M. Carena, J.M. Moreno, M. Quirós, M. Seco and C.E.M. Wagner, *Supersymmetric CP-violating currents and electroweak baryogenesis*, *Nucl. Phys.* **B 599** (2001) 158 [`hep-ph/0011055`];
M. Carena, M. Quirós, M. Seco and C.E.M. Wagner, *Improved results in supersymmetric electroweak baryogenesis*, *Nucl. Phys.* **B 650** (2003) 24 [`hep-ph/0208043`].

[35] J.M. Cline, M. Joyce and K. Kainulainen, *Supersymmetric electroweak baryogenesis*, *JHEP* **07** (2000) 018 [`hep-ph/0006119`].

[36] V. Cirigliano, S. Profumo and M.J. Ramsey-Musolf, *Baryogenesis, electric dipole moments and dark matter in the MSSM*, *JHEP* **07** (2006) 002 [`hep-ph/0603246`].

[37] K. Kainulainen, T. Prokopec, M.G. Schmidt and S. Weinstock, *First principle derivation of semiclassical force for electroweak baryogenesis*, *JHEP* **06** (2001) 031 [`hep-ph/0105295`];
T. Konstandin, T. Prokopec, M.G. Schmidt and M. Seco, *MSSM electroweak baryogenesis and flavour mixing in transport equations*, *Nucl. Phys.* **B 738** (2006) 1 [`hep-ph/0505103`].

[38] S.V. Demidov and D.S. Gorbunov, *Non-minimal split supersymmetry*, *JHEP* **02** (2007) 055 [`hep-ph/0612368`].

[39] WMAP collaboration, D.N. Spergel et al., *Wilkinson Microwave Anisotropy Probe (WMAP) three year results: implications for cosmology*, `astro-ph/0603449`.

[40] V. Barger, P. Langacker and G. Shaughnessy, *Collider signatures of singlet extended Higgs sectors*, *Phys. Rev.* **D 75** (2007) 055013 [`hep-ph/0611239`].

[41] O.J.P. Eboli and D. Zeppenfeld, *Observing an invisible Higgs boson*, *Phys. Lett.* **B 495** (2000) 147 [`hep-ph/0009158`];
K. Mazumdar and A. Nikitenko, CMS internal note 2004/028.

[42] D. Choudhury and D.P. Roy, *Signatures of an invisibly decaying Higgs particle at LHC*, *Phys. Lett.* **B 322** (1994) 368 [`hep-ph/9312347`];
S.G. Frederiksen, N. Johnson, G.L. Kane and J. Reid, *Detecting invisible Higgs bosons at the CERN large hadron collider*, *Phys. Rev.* **D 50** (1994) 4244;
R.M. Godbole, M. Guchait, K. Mazumdar, S. Moretti and D.P. Roy, *Search for 'invisible' Higgs signals at LHC via associated production with gauge bosons*, *Phys. Lett.* **B 571** (2003) 184 [`hep-ph/0304137`];
S.-h. Zhu, *Detecting an invisibly Higgs boson at Fermilab Tevatron and CERN LHC*, *Eur. Phys. J.* **C 47** (2006) 833 [`hep-ph/0512055`].

[43] H. Davoudiasl, T. Han and H.E. Logan, *Discovering an invisibly decaying Higgs at hadron colliders*, *Phys. Rev.* **D 71** (2005) 115007 [`hep-ph/0412269`].

[44] See, for example, B. Heinemann's presentation to the P5 Committee, Fermilab, September 2006, http://hep.ph.liv.ac.uk/~beate/homepage/p5-discovery.pdf.

[45] COMPHEP collaboration, E. Boos et al., *Comphep 4.4: automatic computations from lagrangians to events*, *Nucl. Instrum. Meth.* **A534** (2004) 250 [`hep-ph/0403113`].

[46] LHC/LC STUDY GROUP collaboration, G. Weiglein et al., *Physics interplay of the LHC and the ILC*, *Phys. Rept.* **426** (2006) 47 [`hep-ph/0410364`].

[47] B.K. Gjelsten, D.J. Miller and P. Osland, *Measurement of SUSY masses via cascade decays for SPS 1a*, *JHEP* **12** (2004) 003 [hep-ph/0410303].

[48] W. Beenakker, R. Hopker, M. Spira and P.M. Zerwas, *Squark and gluino production at hadron colliders*, *Nucl. Phys.* **B 492** (1997) 51 [hep-ph/9610490].

[49] B.C. Allanach, C.G. Lester, M.A. Parker and B.R. Webber, *Measuring sparticle masses in non-universal string inspired models at the LHC*, *JHEP* **09** (2000) 004 [hep-ph/0007009].

[50] A. Freitas and P.Z. Skands, *Determining the SUSY-QCD Yukawa coupling*, *JHEP* **09** (2006) 043 [hep-ph/0606121].

[51] LEP collaboration, *Combination procedure for the precise determination of Z boson parameters from results of the LEP experiments*, hep-ex/0101027.

[52] ECFA/DESY LC Physics Working Group collaboration, J.A. Aguilar-Saavedra et al., *TESLA technical design report part III: physics at an e^+e^- linear collider*, hep-ph/0106315.

[53] M. Carena, A. de Gouvea, A. Freitas and M. Schmitt, *Invisible Z-boson decays at e^+e^- colliders*, *Phys. Rev.* **D 68** (2003) 113007 [hep-ph/0308053].

[54] P. Garcia-Abia, W. Lohmann and A. Raspereza, LC-PHSM-2000-062, www-flc.desy.de/lcnotes/.

[55] M. Schumacher, LC-PHSM-2003-096, www-flc.desy.de/lcnotes/.

[56] M. Battaglia and K. Desch, *Precision studies of the Higgs boson profile at the e^+e^- linear collider*, hep-ph/0101165.

[57] A. Freitas, D.J. Miller and P.M. Zerwas, *Pair production of smuons and selectrons near threshold in e^+e^- collisions*, *Eur. Phys. J.* **C 21** (2001) 361 [hep-ph/0106198];
A. Freitas, A. von Manteuffel and P.M. Zerwas, *Slepton production at e^+e^- and e^-e^- linear colliders*, *Eur. Phys. J.* **C 34** (2004) 487 [hep-ph/0310182].

[58] T. Behnke, S. Bertolucci, R.D. Heuer and R. Settles, *TESLA technical design report, Part IV*, DESY-2001-011D.

[59] See, for example, G. Wilson's presentation at *Workshop on the LHC Early Phase for the ILC*, Fermilab, Batavia, Illinois, USA, Apr 12–14, 2007

[60] T. Sjöstrand, S. Mrenna and P. Skands, *Pythia 6.4 physics and manual*, *JHEP* **05** (2006) 026 [hep-ph/0603175].

[61] P. Grannis et al., *ICFA report, Parameters for the Linear Collider*, (2003) www.fnal.gov/directorate/icfa/LC_parameters.pdf.

[62] S.M. Xella Hansen, M. Wing, D.J. Jackson, N. De Groot and C.J.S. Damerell, *Update on flavour tagging studies for the future linear collider using the BRAHMS simulation*, LC-PHSM-2003-061.

[63] K.A. Olive and D. Thomas, *A light dark matter candidate in an extended supersymmetric model*, *Nucl. Phys.* **B 355** (1991) 192.

[64] P. Gondolo et al., *Darksusy: computing supersymmetric dark matter properties numerically*, *JCAP* **07** (2004) 008 [astro-ph/0406204].

[65] S. Katsanevas and P. Morawitz, *SUSYGEN-2.2: a Monte Carlo event generator for MSSM sparticle production at e^+e^- colliders*, *Comput. Phys. Commun.* **112** (1998) 227 [hep-ph/9711417].

[66] R.J. Gaitskell, *Direct detection of dark matter*, *Ann. Rev. Nucl. Part. Sci.* **54** (2004) 315.

[67] V. Barger et al., *Recoil detection of the lightest neutralino in MSSM singlet extensions*, *Phys. Rev.* **D 75** (2007) 115002 [hep-ph/0702036].

[68] http://dmtools.berkeley.edu/limitplots/.

[69] SUPER-KAMIOKANDE collaboration, S. Desai et al., *Search for dark matter wimps using upward through-going muons in super-kamiokande*, *Phys. Rev.* **D 70** (2004) 083523 [*Erratum ibid.* **D 70** (2004) 109901] [hep-ex/0404025].

[70] J. Hisano, K. Kawagoe and M.M. Nojiri, *A detailed study of the gluino decay into the third generation squarks at the CERN LHC*, *Phys. Rev.* **D 68** (2003) 035007 [hep-ph/0304214].

[71] S.K. Lamoreaux, *Solid state systems for electron electric dipole moment and other fundamental measurements*, nucl-ex/0109014.

[72] Y.K. Semertzidis, *Electric dipole moments of fundamental particles*, *Nucl. Phys.* **131** *(Proc. Suppl.)* (2004) 244 [hep-ex/0401016].